ICHEP'98 #210
Submitted to Pa 10
Pl 12

DELPHI 98-138 CONF 199
22 June, 1998

Search for R-parity violating effects at $\sqrt{s} = 183$ GeV

Preliminary

DELPHI Collaboration

R. Barbier [1], **C. Bérat** [2], **M. Besançon** [3], **S. Katsanevas** [1], **C. Mulet-Marquis** [2], **F. Naraghi** [2], **R. Nicolaïdou** [2], **N. Vassilopoulos** [4]

Abstract

Searches for pair production of supersymmetric particles in e^+e^- collisions at center of mass energy of 183 GeV have been performed on DELPHI data under the assumption that R-parity is not conserved and that only one R-parity violating coupling is dominant at a time. Since in these models any particle can be the lightest supersymmetric particle, the searches for charginos, neutralinos, sleptons and squarks have been performed both for direct R-parity violating decays and for indirect cascade decays. All three R-parity violating types of couplings (λ, λ' and λ'') have been studied assuming that the strength of the couplings is such that the lifetimes can be neglected. The pair production of supersymmetric particles is used to constraint domains of the parameter space, previously explored under the assumption of R-parity conservation.

Paper submitted to the ICHEP'98 Conference
Vancouver, July 22-29

[1] IPNL, Lyon (France)
[2] ISN, Grenoble (France)
[3] CEA, Saclay (France)
[4] University of Oxford, Oxford (England)

1 Introduction

1.1 The R-parity violating Lagrangian

In the Minimal Supersymmetric extension of the Standard Model (MSSM) [1], the interactions are consistent with a $B-L$ conservation (B = baryon number, L = lepton number). As a consequence, the MSSM possesses a multiplicative R-parity invariance, where $R=(-1)^{3B+L+2S}$ for a particle with spin S [2]. Standard particles have even R-parity, and the corresponding superpartners have odd R-parity.

One approach to go *beyond the MSSM* is to retain the minimal particle content of the MSSM, but remove the assumption of R-parity invariance. In this scenario, new interactions violating B or L conservation appear, which can be introduced in the superpotential as [3]:

$$\lambda_{ijk}L_iL_j\bar{E}_k+\lambda'_{ijk}L_iQ_j\bar{D}_k+\lambda''_{ijk}\bar{U}_i\bar{D}_j\bar{D}_k$$

where i, j and k are the generation indices; L and E denote the lepton superfields and Q, U, D the quark superfields; λ_{ijk}, λ'_{ijk} and λ''_{ijk} are the new Yukawa couplings. The two first terms violate L conservation, and the third one B conservation. Since $\lambda_{ijk}=-\lambda_{jik}$, $\lambda''_{ijk}=-\lambda''_{ikj}$, there are 9 λ_{ijk}, 27 λ'_{ijk}, 9 λ''_{ikj} leading to 45 new couplings. But all R-parity violating ($\not{R}_p$) terms cannot be simultaneously present, otherwise the proton would rapidly decay [4, 5].

One major phenomenological consequence of $\not{R}_p$ is that the Lightest Supersymmetric Particle (LSP) is allowed to decay to standard fermions. This fact modifies the signatures of the supersymmetric particle production compared to the expected signatures in case of R-parity conservation. Moreover, the single sparticle production is possible. In this paper, the search for pair produced neutralinos ($\widetilde{\chi}_i^0$), charginos ($\widetilde{\chi}^{\pm}$) and sfermions is performed in the hypothesis of R-parity violation with only one dominant coupling (λ,λ',λ'').

In case of pair production of supersymmetric particles, R_p is conserved at the production vertex; the cross section does not depend on the $\not{R}_p$ couplings. On the contrary, the $\not{R}_p$ decay width depends on the λ coupling strength, which then determines the mean decay length of the LSP. If the LSP is a neutralino or a chargino, the mean decay length is given by [6, 7]:

$$L(cm)=0.3\ (\beta\gamma)\left(\frac{m_{\tilde{l}}}{100\mathrm{GeV/c^2}}\right)^4\left(\frac{1\mathrm{GeV/c^2}}{\mathrm{m}_{\widetilde{\chi}}}\right)^5\frac{1}{\lambda^2} \tag{1}$$

where $\lambda=\lambda_{ijk}$, $\sqrt{3}\lambda'_{ijk}$, or $\sqrt{3}\lambda''_{ijk}$, and with $\beta\gamma=P_{\widetilde{\chi}}/m_{\widetilde{\chi}}$. If the LSP is a sfermion, the previous formula becomes:

$$L(cm)=10^{-12}\ (\beta\gamma)\left(\frac{1\mathrm{GeV/c^2}}{\mathrm{m}_{\widetilde{\mathrm{f}}}}\right)\frac{1}{\lambda^2} \tag{2}$$

The condition that the LSP decays close to the production vertex ($L\lesssim 1$ cm) for typical masses considered in this study, implies a lower limit in sensitivity on the λ coupling in the order of $10^{-4}-10^{-5}$ in case of $\widetilde{\chi}^0$, $\widetilde{\chi}^{\pm}$, and 10^{-7} in case of sfermions.

Upper limits on the lambda couplings can be derived from Standard Model processes [8, 9, 10], mainly charged-current universality, lepton universality, $\nu_\mu-e$ scattering, forward-backward asymmetry in e^+e^- collisions, and bounds on ν_e-majorana mass.

1.2 Pair production of neutralinos, charginos and sfermions

The masses and mixing angles of the neutralinos and the charginos are determined by the values of the four parameters M_1, M_2, the U(1) and SU(2) gaugino mass parameters at the electroweak scale, μ, the mixing mass term of the Higgs doublets at the electroweak scale and $tan\beta$, the ratio of the vacuum expectation values of the two Higgs doublets. Assuming that gaugino masses unify at the GUT scale implies $M_1 = \frac{5}{3}\tan^2\theta_W M_2 \simeq \frac{1}{2}M_2$ at the electroweak scale.

The neutralinos and charginos are pair-produced in the s-channel via a γ or a Z, or via a t-channel exchange of a selectron(sneutrino) for the neutralinos(charginos), if the slepton masses are low enough (figure 1). When scans are performed to search for the excluded neutralino mass, we also assume that m_0, the scalar common mass at the GUT scale, determines the slepton masses. When the selectron mass is sufficiently small ($\lesssim$ 100 GeV/c^2), the neutralino production can be enhanced, as the t-channel $\tilde{e}$ exchange dominates the s-channel Z exchange. On the contrary, if the $\tilde{\nu}_e$ mass is in the same range, the chargino cross section can decrease due to destructive interference between the s- and t-channel amplitudes. If the dominant component of neutralinos and charginos is the higgsino ($|\mu| \ll M_2$), the production cross sections are large and insensitive to slepton masses. The appropriate MSSM parameters to consider in the general scan are then M_2, μ, $tan\beta$ and m_0. Depending on the values of the different parameters, the cross sections at $\sqrt{s} = 183$ GeV vary typically from 0.1 to 10 pb.

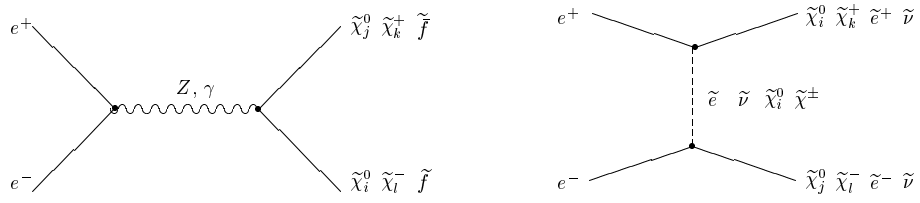

Figure 1: Neutralino, chargino and sfermion pair production diagrams ($i, j = 1, ..4$; $k, l = 1, 2$). Only charged particles are produced via a γ in the s-channel.

The pair production of sneutrinos ($\tilde{\nu}$), charged sleptons ($\tilde{l}$) and squarks ($\tilde{q}$) is also studied. The sfermions can be produced via the exchange in the s-channel of a Z (or a γ for the charged) (figure 1); the production cross section is function of the sfermion mass. In the case of the third generation the mixing angle also enters in the production cross section. The $\tilde{\nu}_e$ ($\tilde{e}$) can also be produced via the exchange of a chargino (neutralino) in the t-channel, and then the cross section depends also on the $\tilde{\chi}^\pm$ ($\tilde{\chi}^0$) mass and through them to the 4 above mentioned MSSM parameters.

1.3 Direct and indirect decays of neutralinos, charginos and sfermions

The decay can be either direct or indirect. In a *direct decay* the sparticle decays directly or via a virtual exchange to standard particles through an $\not{R}_p$ vertex. This is always the case when the sparticle is the LSP. If e.g. the $\tilde{\nu}$ is the LSP, it can decay directly to a pair of fermions through the $\not{R}_p$ operators (see fig. 2). If on the other hand

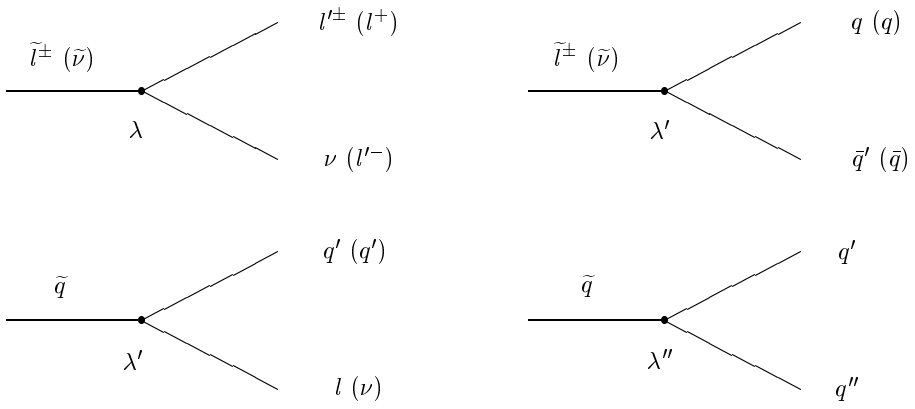

Figure 2: $\not{R}_p$ decays of sfermions.

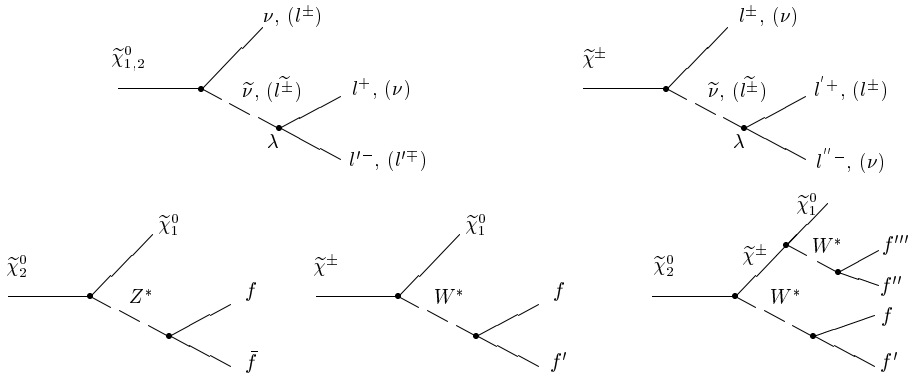

Figure 3: upper part: $\tilde{\chi}^0$ and $\tilde{\chi}^{\pm}$ direct decay via λ coupling, lower part: $\tilde{\chi}^0$ and $\tilde{\chi}^{\pm}$ indirect decay (valid for any coupling).

the lightest neutralino $\tilde{\chi}^o_1$ is the LSP, then it can decay into a fermion virtual-sfermion pair with the subsequent decay of the sfermion to standard fermions via the R-parity violating couplings [1] (see fig. 3).

In an *indirect decay* the sparticle first decays through an R_p-conserving vertex to a standard and on-shell sparticle which then decays through an $\not{R}_p$ vertex. This mode usually dominates when there is enough phase space between "mother" and "daughter" sparticles. As a rule of thumb, when the difference of masses between these 2 sparticles is larger than 5-10 GeV the indirect mode tends to dominate. But regions of the parameter space where one has a "dynamic" suppression of the R_p conserving modes also exist. In this case, even if the sparticle is not the LSP, it decays through an $\not{R}_p$ mode. One has e.g. the case of the light stop decay, where the R_p decay to charm and neutralino is naturally suppressed. A typical example of indirect decay is the R_p decay $\tilde{\chi}^+_1 \rightarrow \tilde{\chi}^0_1 + W^{*+}$ and the subsequent decay of $\tilde{\chi}^0_1$ through the $\not{R}_p$ couplings. In the case of e.g. λ'' dominance, the direct $\tilde{\chi}^+_1$ decay has a signature of 3 jets, while the indirect would give either 5 jets or 3

[1] A complication arises when the decay lifetimes of squarks become larger than the hadronization ones. The system hadronizes into a squark hadron before decay and all the ambiguities in the modelization of the R_p $\tilde{t}$ decay become relevant for the $\not{R}_p$ decays.

jets + 1 lepton + missing energy, depending on the decay modes of W^*.

2 Data samples

The data corresponding to an integrated luminosity of 53 pb^{-1} collected during 1997 by the DELPHI detector [11] at center of mass energy around 183 GeV were analysed. For the analyses depending on electron identification, an integrated luminosity of 50.7 pb^{-1} was used in order to remove events affected by problems occuring in the High-density Projection Chamber (HPC).

Concerning the background, the different contributions coming from the Standard Model processes: $e^+e^- \rightarrow Z\gamma$, $\gamma\gamma$, e^+e^-, $We\nu_e$, Ze^+e^-, W^+W^-, ZZ were considered. For the study of four fermion final states, the PYTHIA [12] generator was used; a cross check was performed using the four-fermion final states generated with EXCALIBUR [13]. Two-photon ($\gamma\gamma$) interactions leading to leptonic final states were generated with the BDK program [14]; the $\gamma\gamma \rightarrow$ hadrons were generated using TWOGAM [15]. The $Z\gamma \rightarrow$ hadrons, $\tau^+\tau^-$ and $\mu^+\mu^-$ event samples were produced by PYTHIA, KORALZ [16] and DYMU3 [17] respectively. For processes such as bhabha scattering and two-photon interactions, biased samples were used. To evaluate signal efficiencies, sparticle production was generated using SUSYGEN [18]. For stop and sbottom generation a specific generator has been used[2].

For the signal study, neutralino and chargino pair productions were considered in several points in the MSSM parameter space, corresponding to different values of $tan\beta$ (from 1 to 30), m_0 (between 20 GeV/c^2 and 500 GeV/c^2), μ (between -200 GeV/c^2 and 200 GeV/c^2) and M_2 (between 0 and 400 GeV/c^2), for both λ couplings considered in the analysis. To study the sneutrino pair production, several signal configurations were generated: a $\tilde{\nu}$ mass range from 50 to 90 GeV/c^2 was covered, with λ_{133} or λ_{122} coupling, and with Br($\tilde{\nu} \rightarrow l^+l^-$)=100%. Events with sneutrino indirect decay were also simulated, for different $\tilde{\nu}$ and $\tilde{\chi}$ masses, in order to cover several ranges of mass difference between sneutrinos and neutralinos. The same type of procedure was applied to simulate charged slepton pair production and to study their direct and indirect decays. Equivalent samples have also been simulated for the two other types of couplings.

All generated signal events were processed with the DELPHI detector simulation program. Some searches used a fast simulation of the detector [19] to generate a few hundred points of the supersymmetric parameter space. The fast simulation has been checked against the full simulation and has been found to agree within a few percent. When fast simulation is used, the efficiencies have been down-scaled with factors obtained from the comparison with full simulation.

[2]See the section 4.3 for further details

3 R_p decays with a dominant λ coupling

In the case of a dominant λ_{ijk} coupling, the sleptons couple to the leptons, and the neutralinos and charginos decay into charged leptons and neutrinos. The decay of the lightest neutralino leads to one neutrino and two charged leptons. The heavier neutralinos and the charginos, depending on their mass difference with $\widetilde{\chi}_1^0$, can either decay directly into 3 standard fermions, or decay to $\widetilde{\chi}_1^0$, via for example virtual Z or W, as illustrated on figure 3 and in table 1. Note that, even if the λ couplings lead to purely leptonic decay modes of the lightest neutralino, the indirect decay of chargino or heavier neutralinos may contain some hadronic activity. In order to cover both the direct and indirect decays of $\widetilde{\chi}_i^0$ and $\widetilde{\chi}^{\pm}$, the analysis has to be sensitive to the final states listed in table 2. If the LSP is a $\tilde{\chi}$ with low mass and high boost, it can escape the detection before decaying. Therefore the assumption of a negligible LSP lifetime restricts the sensitivity of this analysis to $M_{\chi_{LSP}} \gtrsim$ 10 GeV/c^2.

direct decay	$\widetilde{\chi}_1^0 \to \nu l^+ l^-$	$\widetilde{\chi}_2^0 \to \nu l^+ l^-$	$\widetilde{\chi}_1^+ \to \nu\nu l^+$, $l^+ l^- l^+$
indirect decay		$\widetilde{\chi}_2^0 \to Z^*\ \widetilde{\chi}_1^0$, $Z^* \to f\bar{f}$ $\widetilde{\chi}_2^0 \to \widetilde{\chi}_1^0 l^+ l^-$, $\widetilde{\chi}_1^0 \gamma$	$\widetilde{\chi}_1^+ \to W^{*+}\ \widetilde{\chi}_1^0$, $W^{*+} \to f\bar{f}'$ $\widetilde{\chi}_1^+ \to \widetilde{\chi}_1^0 \nu_l l^+$

Table 1: Possible decays of neutralinos and charginos when a λ coupling is dominant.

final states	direct decay of	indirect decay of
$2l + \not{E}$	$\widetilde{\chi}_1^+ \widetilde{\chi}_1^-$	
$4l + \not{E}$	$\widetilde{\chi}_1^0 \widetilde{\chi}_1^0$, $\widetilde{\chi}_1^+ \widetilde{\chi}_1^-$	$\widetilde{\chi}_2^0 \widetilde{\chi}_1^0$
$6l$	$\widetilde{\chi}_1^+ \widetilde{\chi}_1^-$	
$6l + \not{E}$		$\widetilde{\chi}_1^+ \widetilde{\chi}_1^-$, $\widetilde{\chi}_2^0 \widetilde{\chi}_1^0$
$4l + 2$ jets $+ \not{E}$		$\widetilde{\chi}_2^0 \widetilde{\chi}_1^0$
$4l + 4$ jets $+ \not{E}$		$\widetilde{\chi}_1^+ \widetilde{\chi}_1^-$
$5l + 2$ jets $+ \not{E}$		$\widetilde{\chi}_1^+ \widetilde{\chi}_1^-$

Table 2: Final states in $\widetilde{\chi}_i^0$, $\widetilde{\chi}^{\pm}$ pair production when a λ coupling is dominant.

The pair production of sneutrinos ($\tilde{\nu}$) and charged sleptons ($\tilde{l}$) is also studied, since a dominant λ coupling allows them to decay into standard leptons and neutrinos. If the $\tilde{\nu}$ is the LSP, with a mass lower or very close to that of the $\widetilde{\chi}_1^0$ or $\widetilde{\chi}^{\pm}$ mass, it decays directly in two leptons with no missing energy. If it is not the LSP, the indirect decays $\tilde{\nu} \to \widetilde{\chi}_1^0 \nu$, $\tilde{\nu} \to \widetilde{\chi}_2^0 \nu$, $\tilde{\nu} \to \widetilde{\chi}^{\pm} l^{\mp}$ are allowed, depending on the MSSM parameters; the $\widetilde{\chi}_2^0$ and $\widetilde{\chi}^{\pm}$ could also decay directly or indirectly, as previously explained. It could also happen that, from a $\tilde{\nu}$ pair, one $\tilde{\nu}$ decays directly and the second indirectly, giving a so-called "mixed decay".

The direct decay of a charged slepton with a λ_{ijk} coupling gives a charged lepton plus a neutrino, while the indirect decay $\tilde{l} \to \widetilde{\chi}_1^0 l$ is dominant in most the MSSM parameter space. In this last case, the final state consists in 6 charged leptons plus missing energy. A mixed decay (one charged slepton decaying directly, the other one indirectly) is also possible. The final states resulting from slepton pair production are listed in table 3.

Decay type		Pair production signature
Direct	$\tilde{\nu} \to l^+ l^-$	$4l$
Indirect	$\tilde{\nu} \to \nu\ \tilde{\chi}_1^0$	$4l + \not{E}$
	$\tilde{\nu} \to \nu\ \tilde{\chi}_2^0$	same as $\tilde{\chi}$ analyses
	$\tilde{\nu} \to l^\pm\ \tilde{\chi}^\pm$	multilepton or lepton+jets
Direct	$\tilde{l}^\pm \to l^\pm \nu$	$2l$(acoplanar)$+\not{E}$
		(like R_p signal $\tilde{l}^\pm \to l^\pm\ \tilde{\chi}_1^0$with $M_{\tilde{\chi}^0}$=0)
Indirect	$\tilde{l}^\pm \to l^\pm\ \tilde{\chi}_1^0$	same as $\tilde{\chi}$ analyses
	$\tilde{l}^\pm \to \nu\ \tilde{\chi}^\pm$	with $\leq$ 2 extra leptons or $\not{E}$

Table 3: Final states in charged slepton and sneutrino pair production when a λ coupling is dominant.

The indirect squark decays into a quark and a neutralino, (such as $\tilde{t} \to\ c\tilde{\chi}_1^0$) where the neutralino decays via a λ coupling, is not considered in this paper.

For all the analyses presented in this section, it was assumed that only one λ_{ijk} is dominant. Two kinds of searches have been performed:

- the first assuming that λ_{122} is dominant. In this case, the charged leptons coming from $\not{R}_p$ decay are muons and electrons. $\tilde{\chi}_1^0$ can decay into $e\nu_\mu\mu$ ($\approx$ 50%), or $\mu\nu_e\mu$ ($\approx$ 50 %); then the corresponding final state for $\tilde{\chi}_1^0$ pair production is: missing energy, coming from the undetected neutrinos, plus $2e2\mu$ ($\approx 25\%$) or $1e3\mu$ ($\approx 50\%$) or 4μ ($\approx 25\%$). This case should have the best efficiency since selection depends on e and μ identification.

- the second assuming that λ_{133} is dominant, meaning that the leptons from $\not{R}_p$ decay are mainly taus, and electrons. This case should have the worst efficiency due to the presence of several τ in the final state.

The other λ_{ijk} couplings lie between these two extreme cases.

Most present indirect limits on the λ couplings are in the range of 10^{-3} to 10^{-1} as it can be seen in table 4 based on [10]. The most stringent upper limit is given for λ_{133}.

ijk	$\lambda_{ijk} \leq$	ijk	$\lambda_{ijk} \leq$	ijk	$\lambda_{ijk} \leq$
$\lambda_{\nu_e\mu e}/\lambda_{e\nu_\mu e}(121)$	0.05	$\lambda_{\nu_e\tau e}/\lambda_{e\nu_\tau e}(131)$	0.06	$\lambda_{\nu_\mu\tau e}/\lambda_{\mu\nu_\tau e}(231)$	0.06
$\lambda_{\nu_e\mu\mu}/\lambda_{e\nu_\mu\mu}(122)$	0.05	$\lambda_{\nu_e\tau\mu}/\lambda_{e\nu_\tau\mu}(132)$	0.06	$\lambda_{\nu_\mu\tau\mu}/\lambda_{\mu\nu_\tau\mu}(232)$	0.06
$\lambda_{\nu_e\mu\tau}/\lambda_{e\nu_\mu\tau}(123)$	0.05	$\lambda_{\nu_e\tau\tau}/\lambda_{e\nu_\tau\tau}(133)$	0.003	$\lambda_{\nu_\mu\tau\tau}/\lambda_{\mu\nu_\tau\tau}(233)$	0.06

Table 4: Indirect limits [10] on the $\not{R}_p$ λ couplings in units of $(m_{\tilde{f}}/100\ \mathrm{GeV}/c^2)$, where $m_{\tilde{f}}$ is the appropriate sfermion mass.

The λ parameters, when simulating signal events, have been set to their present experimental upper limits: $\lambda_{122} = 0.04$ and $\lambda_{133} = 0.003$.

3.1 Neutralinos and charginos decaying through λ

As already mentioned, the indirect decays of neutralinos or charginos can give two or more jets in the final state. Moreover, in case of the λ_{133} coupling, the τ decays give isolated leptons or thin jets. The DURHAM [20] algorithm is used to reconstruct the jets. In order to cover the different topologies, the jet number is not fixed, and the jet charged multiplicity can be low (thin jets with one track are possible), or can be 0 in case of neutral jets. For each event, DURHAM is applied to reconstruct from 2 to 8 jets, and the corresponding jet parameters are stored. The analyses described below are designed to cover all the final states listed in table 2 as well as final states produced when the chargino is the LSP except the $2l+\not{E}$ topology coming from the direct chargino decays, as the region in the MSSM parameter space where this decay dominates is already covered by other studied processes.

3.2 λ_{122} case

Events are selected if they satisfy the following criteria:

- The charged multiplicity has to be greater than 3 as the minimum number of charged tracks expected in these topologies is 4.
- The missing p_t is greater than 5 GeV/c and the polar angle of the missing momentum is between 20 and 160 degrees.
- At least two well identified (standard or tight)[11] muons are required.
- The energy of the most energetic identified lepton must be greater than 20 GeV.
- An isolation criterium is imposed for the identified leptons (no other charged particle in a half cone of 7 degrees around the lepton).
- At least two of the identified leptons must be leading particles in the jets.
- The polar angle of the jets in case of 4, 5 or 6 jet topologies must be between 20 and 160 degrees.
- The missing energy is at least $20\%\sqrt{s}$.

After the cuts, no event remains, while 0.7 events are expected from Standard Model processes, most of which come from W^+W^-. For $\tilde{\chi}_1^0\tilde{\chi}_1^0$ the selection efficiencies are in the range 45-60 %, for $\tilde{\chi}_1^+\tilde{\chi}_1^-$: 20-50%, and for $\tilde{\chi}_2^0\tilde{\chi}_1^0$: 25-40%, for all the values of μ, M_2 planes considered (see table 7).

3.3 λ_{133} case

The τ decay gives isolated leptons or thin jets, plus neutrinos. In this case the missing energy is expected to be higher than in the λ_{122} case due to the presence of neutrinos, coming not only from neutralinos or charginos $\not{R}_p$ decay, but also from τ decay.

Events are pre-selected if they satisfy the following criteria:

- at least one (loose) lepton is identified;
- the number of charged tracks must be greater than 3
- the total energy and the energy from charged particles must be greater than $0.18\sqrt{s}$ and $0.16\sqrt{s}$ respectively.

These cuts remove around 99% of two-photon events.

Several criteria are based on the missing quantities:

- the missing p_t is greater than 5 GeV/c;

- the polar angle of the missing momentum is between 27 and 153 degrees;
- the missing energy is at least $0.30\sqrt{s}$.

These cuts are efficient to suppress the background coming from bhabha, two-photons and Zγ events.

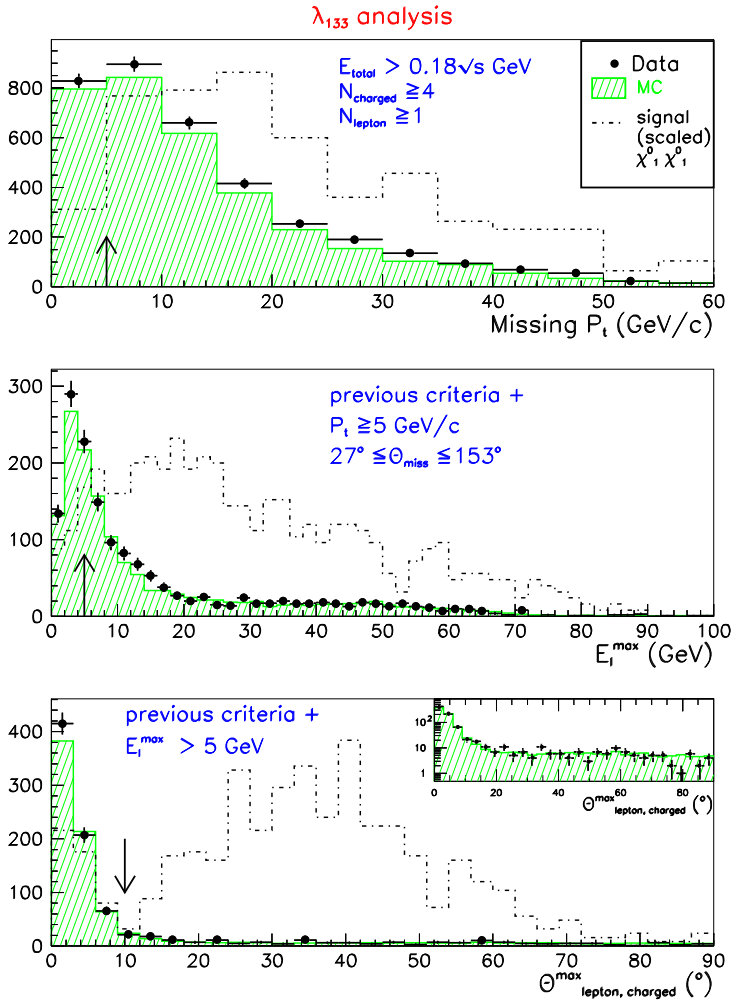

Figure 4: Neutralino and chargino search with a dominant λ coupling: missing transverse momentum, energy of the most energetic lepton and isolation angle distributions for real data (black dots), expected SM background (hatched) and $\widetilde{\chi}_1^0\widetilde{\chi}_1^0$ signal (dotted line). The signal distribution has been scaled (see text). The arrows show the applied cuts.

For the events with less than 8 charged particles, at least one loose lepton is required, whereas events with 8 or more charged particles must have at least two loose leptons. In both cases, the energy of the most energetic lepton must be greater than 5 GeV, and there should be no other charged track in a 10 degree half cone around the identified lepton(s). These last criteria remove Zγ, and hadronic ZZ and W^+W^- events. In figure 4 the distributions of the missing p_t, the energy of the most energetic lepton, and the minimum angle between the lepton and the nearest charged particle, are presented. The agreement between real data and simulated background is fairly good. The distribution for simulated signal ($\widetilde{\chi}_1^0\widetilde{\chi}_1^0$) is also plotted; it is scaled by a factor of ~ 10.

The final selection is based on the jet characteristics and topologies. First, the Y_{34}[3]

[3]The Y_{34} is the transition value of the "Y_{cut}" DURHAM distance in which the event flips from 4 to 3

Selection criteria for λ_{133}coupling	data	MC
at least one loose lepton $N_{charged} \geq 4$ $E_{tot} \geq 18\%\sqrt{s}$, $E_{charged} \geq 16\%\ \sqrt{s}$ missing $p_t > 5$ GeV/c, $27^o \leq \Theta_{miss} \leq 153^o$	1551	1479
$E^l_{max} \geq 5$ GeV	996	965
$\Theta^{min}_{lepton-track} \geq 10^o$	293	286
E_{miss} >30%$\sqrt{s}$	174	166
if $N_{charged} \geq 8, N_{lepton} \geq 2$	70	69.2
$E^{30^o}_{cone} \leq 50\%\ E_{total}$ $Y_{34} \geq 0.001$	33	29.5
in case of 4 or 5 jets, at least 4 charged jets	14	17.9
case of 4 jets: $E^j_{min} * \theta^{j1,j2}_{min} \geq 0.5$GeV rad, $E^j_{min} * \theta^{j1,j2}_{min} \geq 5$ GeV rad if $N_{charged} > 8$ $20^o \leq \theta_{jet} \leq 160^o$	3	3.3

Table 5: List of selection criteria for λ_{133} case.

data	MC	$Z\gamma$	Zee	W^+W^-	ZZ
3	3.3±0.3	0.13±0.01	0.14±0.01	2.73±0.23	0.31±0.05

Table 6: SM background contributions.

value must be greater than 10^{-3}, which reduces the Zγ contribution (figure 5). In case of 4 or 5 jet topologies, 4 charged jets are required. In case of a 4 jet topology, a cut is applied on the value of $E^j_{min} \times \theta^{j_a j_b}_{min}$ where E^j_{min} is the energy of the less energetic jet, and $\theta^{j_a j_b}_{min}$ is the minimum angle between 2 jets. These requirements significantly reduce the Zγ, $\gamma\gamma$, W^+W^- background. The number of remaining real and simulated data events after these cuts are reported in table 5.

For $\tilde{\chi}^0_1\tilde{\chi}^0_1$ the selection efficiencies are in the range 22-34 %, for $\tilde{\chi}^+_1\tilde{\chi}^-_1$: 20-37%, and for $\tilde{\chi}^0_2\tilde{\chi}^0_1$: 20-25%, for all the μ, M_2 planes considered. 3 events remain after the selection procedure with 3.3 expected from standard background processes. The background is mainly due to W^+W^- events (table 6).

The results obtained for both λ_{122} and λ_{133} coupling are summarized in table 7.

3.4 Sneutrinos decaying through λ

The final state in $\tilde{\nu}\tilde{\nu}$ production is typically purely leptonic. It is the case either for direct decay ($4l$), or for the dominant indirect decay via the lightest neutralino ($4l+\not{E}$). The last decay is the indirect dominant mode since the negative chargino search results (see section 3.6) imply that the indirect decay to $\tilde{\chi}^{\pm}l^{\mp}$ is negligible for a $\tilde{\nu}$ with a mass lower than 90 GeV/c^2.

To be more efficient for all these purely leptonic final states, with at least 4 leptons, the selection criteria have been strengthened with respect to the chargino/neutralino analyses.

jet configuration.

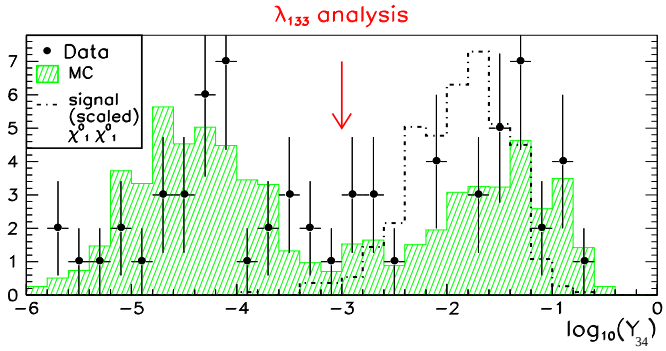

Figure 5: Neutralino and chargino search with a dominant λ coupling: $log_{10}(Y_{34})$ distribution for real (black dots) and expected SM background (hatched histogram). A scaled (see text) signal distribution is also plotted to show that the applied cut removes less than 1% of the signal, and half of the background.

Coupling	process	Efficiency range in %	Selected events data	Selected events MC
λ_{122}	$\tilde{\chi}_1^0\tilde{\chi}_1^0$	45-60	0	0.7±0.1
	$\tilde{\chi}_2^0\tilde{\chi}_1^0$	25-40		
	$\tilde{\chi}_1^+\tilde{\chi}_1^-$	20-50		
λ_{133}	$\tilde{\chi}_1^0\tilde{\chi}_1^0$	22-34	3	3.3±0.3
	$\tilde{\chi}_2^0\tilde{\chi}_1^0$	20-25		
	$\tilde{\chi}_1^+\tilde{\chi}_1^-$	20-37		

Table 7: Neutralino and chargino analyses (λ couplings): efficiency ranges for pair production processes, and data and Monte-Carlo events selected for each studied coupling.

In case of λ_{122} coupling, the best selection efficiency is obtained from the direct decays as described below; the indirect decays have not been simulated since they lead to final states already covered by the analyses explained before and since the most conservative results are obtained with λ_{133} coupling. In case of λ_{133} coupling, the same analysis is used to study both direct and indirect decays since they lead to the same final state with more or less missing energy.

3.4.1 λ_{122} case

If λ_{122} is the dominant $\not{R}_p$ coupling, the direct decay mode leads to 4 leptons (μ or/and e) in the final state. The selection criteria are described below:

- the charged multiplicity has to be 4;
- at least 2 well identified muons[11] are required;
- the total energy from charged particles has to be greater than $33\%\sqrt{s}$;
- no other charged particle in a half cone of 10 degrees around the lepton, is demanded;
- the sum of the total event charge has to be 0;
- the missing energy has to be less than $55\%\sqrt{s}$;
- the thrust value has to be less than 0.95.

No event remains in the data after these cuts with 0.8 expected from standard background processes. The efficiencies were evaluated by generating sneutrino pair production with masses from 50 to 90 GeV/c^2 and they are in the range of 60-80% depending on the sneutrino mass (table 9).

3.4.2 λ_{133} case

The preselection criteria are the same as in case of chargino/neutralino studies, except that an upper limit of 8 is set on the number of charged tracks, which eliminates more than 90% of all Standard Model backgrounds. A lower cut on the missing energy can be applied even in case of $4l$ final states, due to the τ decay which produces a certain amount of missing energy. But compared to the neutralino decay in which neutrinos are produced directly, the missing energy is less important, therefore the limit is set to $0.1\sqrt{s}$. The missing longitudinal momentum must be lower than 70 GeV/c.

The criteria applied for the identified lepton(s) are also modified. If there are exactly 4 charged tracks, the minimum angle between a lepton and the nearest charged track must be greater than 20 degrees, otherwise it must be greater than 6 degrees.

As for the chargino/neutralino selection, several criteria are based on the jet characteristics. The DURHAM Y_{34} and Y_{45} values (see section 3.3) must be respectively greater than $1.8 \cdot 10^{-3}$ and $4 \cdot 10^{-4}$. In case of a 4 jet topology, there must be no neutral jet, at least one jet with its leading track identified as a lepton, and a minimum angle of 20 degrees between 2 jets. The value of $E^j_{min} \times \theta^{j_a j_b}_{min}$ must be greater than 1 GeV rad, and than 4 GeV rad if $N_{charged} = 8$.

One event remains after this selection with 1.8 expected from standard background processes. The background is mainly due to W^+W^-, $\gamma\gamma$ and ZZ events (table 8).

data	MC	$\gamma\gamma$	Zee	W^+W^-	ZZ
1	1.81±0.21	0.57±0.17	0.14±0.01	0.67±0.11	0.42±0.07

Table 8: Main SM background contributions in the sneutrino analysis, in case of λ_{133} coupling.

In the indirect decay $\tilde{\nu} \rightarrow \nu\tilde{\chi}^0_1$ the final state depends on the λ_{ijk} coupling, since the charged leptons are produced in the $\tilde{\chi}^0_1$ $\not{R}_p$ decay. Therefore the efficiencies do not depend on the sneutrino type, but on the sneutrino and neutralino masses. The selection efficiencies are summarized in table 9.

3.5 Charged sleptons decaying through λ

For most of the MSSM parameter space studied, the indirect decay of sleptons[4] in $l\tilde{\chi}^0_1$ is dominant; only in some particular regions, the staus have a non negligeable branching fraction into $\nu\tilde{\chi}^{\pm}$, but this region is excluded by our present limit on the chargino mass. The indirect slepton decay gives mostly purely leptonic final state. A particular analysis is devoted to the case of the direct decay of the slepton pair, leading to $2l+\not{E}$ final state.

[4]in this section the term "slepton" means charged slepton

coupling	process	characteristics	efficiency range in %	selected events data	selected events MC
λ_{122}	$\widetilde{\nu}_e \to \mu^+\mu^-$	direct decay	60-80	0	0.8±0.1
	$\widetilde{\nu}_\mu \to e^\pm\mu^\mp$	direct decay	50-70		
λ_{133}	$\widetilde{\nu}_e \to \tau^+\tau^-$	direct decay	32-37	1	1.8±0.2
	$\widetilde{\nu}_\tau \to e^\pm\tau^\mp$	direct decay	41-47		
	$\tilde{\nu} \to \widetilde{\chi}_1^0\nu$	$20 < \widetilde{\chi}_1^0$mass < 30	18-29		
		$30 < \widetilde{\chi}_1^0$mass < 40	27-36		
		$40 < \widetilde{\chi}_1^0$mass	35-39		

Table 9: Sneutrino analysis: efficiency ranges in the different studied cases, and data and Monte-Carlo events remaining after the applied selection. Sneutrinos were generated with masses in the range 50-90 GeV/c^2

• **Analysis concerning the direct slepton decays**

With λ_{133} coupling, only the $\tilde{\tau}$ can decay directly, and it has 2 decay modes: $\tilde{\tau} \to \tau\nu_e$ (50%), $\tilde{\tau} \to e\nu_\tau$ (50%). Then the final state in pair production of $\tilde{\tau}$ is: missing energy + ee (25%), $e\tau$ (50%), $\tau\tau$ (25%). Three specific analysis are performed for the 3 components of the final state. Several preselection criteria are common to the $2e+\not{E}$ and $e\tau+\not{E}$ analysis:

- the missing p_t must be greater than 20 GeV/c and the polar angle of the missing momentum must between 25 and 155 degrees;
- the acolinearity must be greater than 10 degrees, and the acoplanarity must be less than 160 degrees;
- the energy of the most energetic photon must be less than 10 GeV.

Then different criteria are applied to discriminate the 2 channels:

$ee+\not{E}$ final state

- 2 loose electrons are required; the angle between them must be at least 10 degrees and at most 160 degrees;
- the energy of each electron must be greater than 10 GeV, and the sum of their energy less than 110 GeV;
- the neutral multiplicity of the event must be less than 2.

$e\tau+\not{E}$ final state

- the charged multiplicity and the neutral multiplicity must be both less than 5;
- at least one loose electron is required, and not more than one identified muon;
- if there is one identified muon, the charged multiplicity must be 2 (one μ, one e);
- the sum of the total event charge has to be 0;
- the total energy from charged particles has to be greater than $5\%\sqrt{s}$ and lower than $65\%\sqrt{s}$
- the minimum angle between the lepton and the closest charged particle must be at least 10 degrees, at most 160 degrees, and the minimum angle between the lepton and the nearest neutral must be greater than 10 degrees;
- the total electromagnetic energy must be at least 10 GeV, and the total leptonic energy must be between 10 and 110 GeV

The results of these 2 analyses are summarized in table 10.

channel	efficiencies (%) as function of stau							selected events	
	mass(GeV/c^2): 50	55	60	65	70	75	80	data	background
$ee+\not{E}$	30	32	35	33	35	41	40	0	1.3
$e\tau+\not{E}$	19	21	22	22	22	27	29	1	2.8

Table 10: Slepton direct decay: efficiencies for several values of $\tilde{\tau}$ masses and data and Monte-Carlo events remaining after the applied selection, for both channels.

For the $\tau\tau+\not{E}$ final state the analysis performed for the search of R_p conserved $\tilde{\tau} \rightarrow \tau\ \tilde{\chi}_1^0$ decay [21] has been used: 7 events are selected for 7.5 expected, with an efficiency of 31% which is rather stable in the $\tilde{\tau}$ mass range considered.

- **Analysis concerning the indirect slepton decays**

In the case of λ_{122} analysis, the most efficient case is studied, namely the indirect smuon decay; the selection criteria consist of:

- charged multiplicity greater or equal to 4,
- at least 3 well identified muons,
- the total leptonic energy greater than 80 GeV.

In case of λ_{133} analysis, the same criteria used for the sneutrino searches are applied. But, contrary to the $\tilde{\nu}$ case, for any given type of coupling, the selection efficiencies depend on the slepton family since in the final state, there is always a lepton of the same flavour. Selection efficiencies depend also on slepton and neutralino masses. Efficiencies and results are reported in table 11.

coupling	process	$\tilde{\chi}_1^0$ mass range in GeV/c^2	efficiency range in %	selected events data	selected events MC
λ_{122}	$\tilde{\mu} \rightarrow \mu\tilde{\chi}_1^0$	50-80	70-80	0	0.3±0.1
λ_{133}	$\tilde{e} \rightarrow e\tilde{\chi}_1^0$	50-80	35-39	1	1.8
	$\tilde{\mu} \rightarrow \mu\tilde{\chi}_1^0$	50-80	42-48		
	$\tilde{\tau} \rightarrow \tau\tilde{\chi}_1^0$	25-35	24-29		
		35-45	25-32		
		45-80	26-34		

Table 11: Slepton analyses: efficiency ranges in the different studied cases, and data and Monte-Carlo events remaining after the applied selection. Sleptons were generated with masses in the range 50-90 GeV/c^2.

3.6 Interpretation of λ dominant searches in terms of MSSM parameters

By performing the analysis described in the previous sections at $\sqrt{s} = 183$ GeV, no excess of events was found in the data with respect to the Standard Model expectation. As a consequence, limits on the production and mass of the charginos and neutralinos can be

set. Both direct and indirect decays of pair production of charginos and neutralinos are combined to give the exclusion contours at 95% C.L. in the μ, M_2 plane.

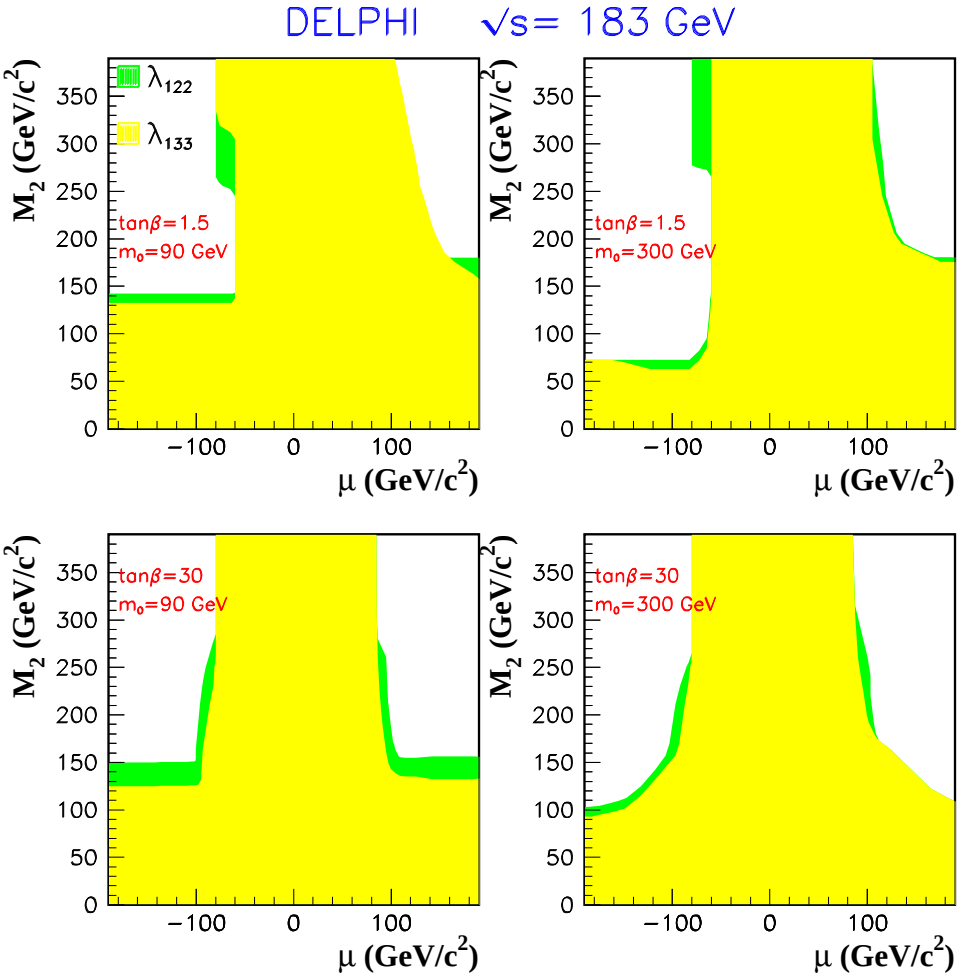

Figure 6: Neutralino and chargino searches with a dominant λ coupling: regions in μ, M_2 parameter space excluded at 95 % C.L. for two values of $tan\beta$ and two values of m_0. The exclusion area obtained from the λ_{133} search is shown in light grey and the corresponding area for the λ_{122} search is shown in dark grey. The second exclusion area includes the first. The data collected at E_{CM} = 183 GeV are used.

For each coupling, the analysis is sensitive to most of the possible decay channels of neutralinos and charginos produced in the three processes considered ($\tilde{\chi}^0_1\tilde{\chi}^0_1$, $\tilde{\chi}^0_2\tilde{\chi}^0_1$, $\tilde{\chi}^+_1\tilde{\chi}^-_1$). Then, the number of expected events N_{exp}, for a given set of MSSM parameters is

$$N_{exp} = \mathcal{L} \times \sum_{i=1}^{i=3} \epsilon_i \sigma_i$$

where ϵ_i gives the efficiency for each process, σ_i the corresponding cross section and $\mathcal{L}$ the integrated luminosity. The maximum number of signal events N_{95} in presence of background is given by the standard formula [22]. All the points in the μ, M_2 plane which satisfy the condition $N_{exp} > N_{95}$ are excluded at 95% C.L. The exclusion contours for two values of $tan\beta$ and m_0 are shown on figure 6. The light grey area shows the region

excluded by the λ_{133} search and the dark grey area the region excluded by the λ_{122} search which, having a better efficiency, includes and extends the excluded region. One can consider these two searches as the most and the least sensitive cases. The other couplings have a sensitivity lying in between these two extremes. This result can be translated into a lower limit on neutralino mass as shown in the figure 7, which was obtained by scanning over m_0 values for each $tan\beta$ in order to set a limit independantly of the choice of m_0. With this search, neutralinos with masses less than 27 GeV/c^2 are excluded at 95 % C.L. whereas the corresponding limit for charginos is 89 GeV/c^2.

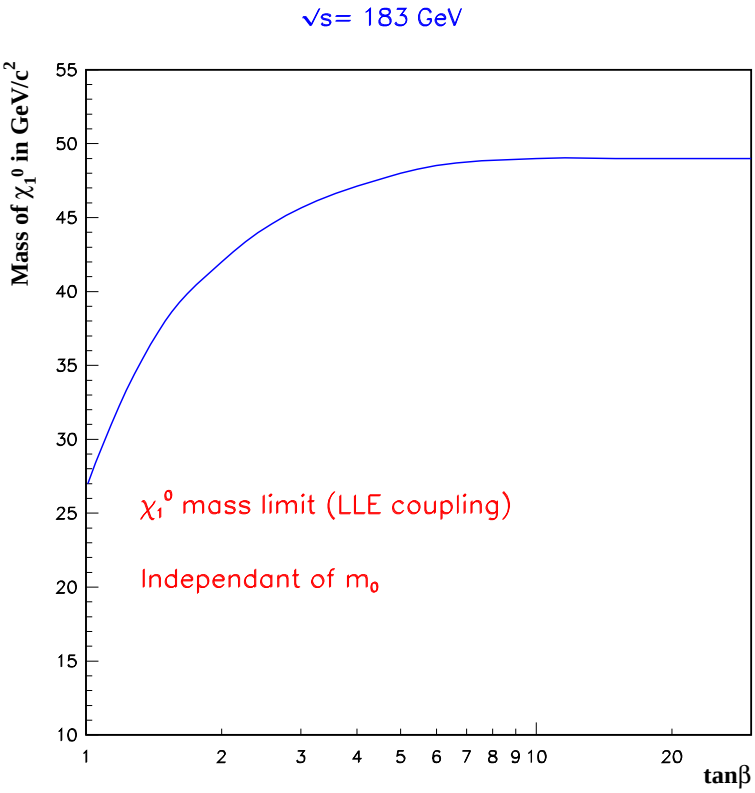

Figure 7: The lightest neutralino mass as a function of $tan\beta$ at 95 % confidence level. This limit is independent of the choice of m_0 and the generation indices i,j,k of the λ_{ijk} coupling.

A sneutrino can decay either directly into two charged leptons, or indirectly into a neutralino and a neutrino; the decay to chargino+lepton is kinematically inaccessible for a sneutrino mass up to $\simeq$ 90 GeV/c^2.

For any given λ_{ijk} coupling, only the $\tilde{\nu}_i$ and $\tilde{\nu}_j$ can decay directly into 2 charged leptons and have only one possible direct decay mode. In case of λ_{122} coupling, the final states are $\mu\mu\mu\mu$ ($\tilde{\nu}_e$ pair) or $ee\mu\mu$ ($\tilde{\nu}_\mu$ pair); in case of λ_{133} coupling, the final states are $\tau\tau\tau\tau$ ($\tilde{\nu}_e$ pair) or $ee\tau\tau$ ($\tilde{\nu}_\tau$ pair). The 4 τ final state is also possible in case of $\tilde{\nu}_\mu$ pair decaying with a λ_{233} coupling. The efficiencies obtained for these channels, for different values of the sneutrino mass, combined with the results of the selection on data and background, allow to derive a limit on the cross section as a function of the $\tilde{\nu}$ mass, shown on figure 8. On the same plot the MSSM cross sections of $e^+e^- \rightarrow \tilde{\nu}\tilde{\nu}$ versus the $\tilde{\nu}$ mass are reported; in the case of $\tilde{\nu}_\mu$ and $\tilde{\nu}_\tau$, the pair production cross section depends only on the $\tilde{\nu}$ mass; in

case of $\tilde{\nu}_e$, it may have a dependance on the MSSM parameters since it depends on the mass of the chargino exchanged in the t-channel. When the chargino mass is greater than 400 GeV/c^2, $\sigma(e^+e^- \rightarrow \tilde{\nu}_e\tilde{\nu}_e) = \sigma(e^+e^- \rightarrow \tilde{\nu}_\mu\tilde{\nu}_\mu)$. The dashed upper curve on the plot is the cross section obtained with a chargino mass $\simeq$ 90 GeV/c^2. From this figure, one can see that the limit on the mass of a sneutrino decaying directly into 2 leptons is 63 GeV/c^2.

The indirect decay of the sneutrino into a neutrino and a neutralino gives the same signature as the neutralino $\not{R}_p$ decay with the bonus of extra missing energy. It does not depend on the sneutrino flavour, but only on the λ_{ijk} coupling. As for the charginos/neutralinos, the most conservative limit is obtained from the λ_{133} coupling. Taking into account the efficiencies obtained for several values of sneutrino and neutralino masses, and the analysis results, an exclusion area is determined in the $m_{\tilde{\nu}}$, $m_{\tilde{\chi}^0_1}$ plane (figure 9). The largest exclusion area is obtained for $e^+e^- \rightarrow \tilde{\nu}_e\tilde{\nu}_e$, with a chargino mass close to the kinematic limit. The smallest exclusion area is obtained from $\tilde{\nu}_\mu\tilde{\nu}_\mu$,$\tilde{\nu}_\tau\tilde{\nu}_\tau$, and is also valid for $\tilde{\nu}_e\tilde{\nu}_e$ in case of a heavy chargino. Since the efficiencies are lower for the light neutralinos, the exclusion domain is reduced compared to heavier neutralinos. Taking into account the limit of the neutralino mass at 27 GeV/c^2, the lower bound on sneutrino mass is 62 GeV/c^2, in the case of indirect decay. On the same plot the limits obtained in case of direct decay are reported. The line labelled λ_{233} corresponds to $\tilde{\nu}_\mu$ pair production leading to a 4 τ final state. This limit is lower than the one obtained for the indirect decay into $\tilde{\chi}^0_1\nu$ when $m_{\tilde{\chi}^0}$ is greater than 30 GeV/c^2 and with a λ_{133} coupling, since in this case the final state is a mixing of $4\tau, 1e3\tau, 2e2\tau$, and the efficiency is slightly higher. According to these results, a sneutrino lower than 62 GeV/c^2 is excluded at 95% C.L.

A slepton can decay either directly into a charged lepton and a neutrino, or indirectly into a neutralino and a charged lepton; the decay to chargino+neutrino is kinematically inaccessible for a slepton mass up to $\simeq$ 90 GeV/c^2. Right handed sleptons have been studied here, because their production cross section is lower than the left handed one, therefore leading to more conservative results.

For the direct searches, the results obtained from the 3 analyses described in section 3.5 are combined and limits on the production cross section as a function of slepton mass is derived at 95% C.L (figure 10). Considering the MSSM cross section a limit on the slepton mass is set at $m_{\tilde{l}}$ >61 GeV/c^2.

For the indirect searches, the most conservative limit is obtained considering the λ_{133} coupling as stated before. With the results of the analyses described in section 3.5, an exlusion region is derived in the $m_{\tilde{l}}$, $m_{\tilde{\chi}^0_1}$ plane (figure 11). Direct topologies lead to worst limits on slepton masses as the remaining background is higher than in case of indirect ones. Therefore our present limit on slepton mass is $m_{\tilde{l}}$ >61 GeV/c^2.

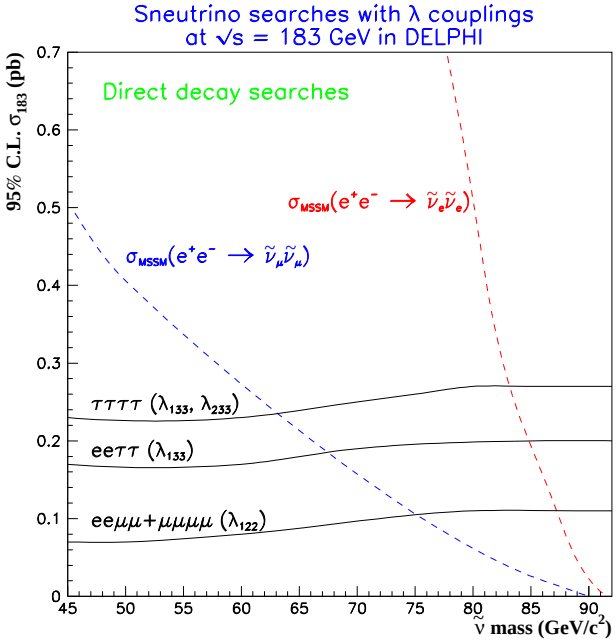

Figure 8: Sneutrino direct decay with λ coupling: the limit on the $\tilde{\nu}\tilde{\nu}$ production cross section as a function of the mass is plotted for different final states. The MSSM cross sections are reported, in order to derive a limit on the sneutrino mass in case of direct $\not{R}_p$ decay. The dashed upper curve on the plot is the $\tilde{\nu}_e\tilde{\nu}_e$ cross section obtained with a chargino mass $\simeq 90$ GeV/c^2.

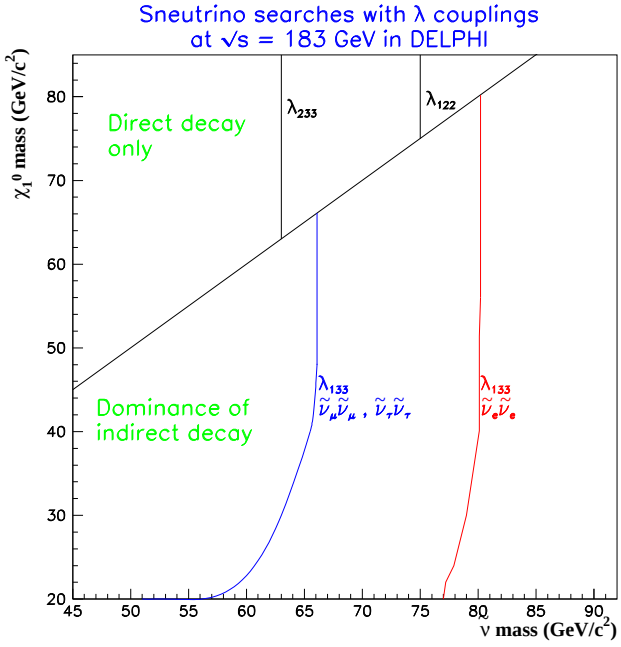

Figure 9: Sneutrino search with λ coupling: exclusion domain in $m_{\tilde{\chi}^0}$ versus $m_{\tilde{\nu}}$ for the $\tilde{\nu}$ pair production cross section; the diagonal line separates the plot in 2 regions: in the upper part, only the direct decay is allowed; in the lower part, the indirect decay is dominant, so the exclusion limit depends also on the neutralino mass. In both cases, only the most conservative limit has been reported, for the $\tilde{\nu}_\mu$ and $\tilde{\nu}_\tau$ production, and for the $\tilde{\nu}_e$ in case of chargino mass close to the kinematic limit.

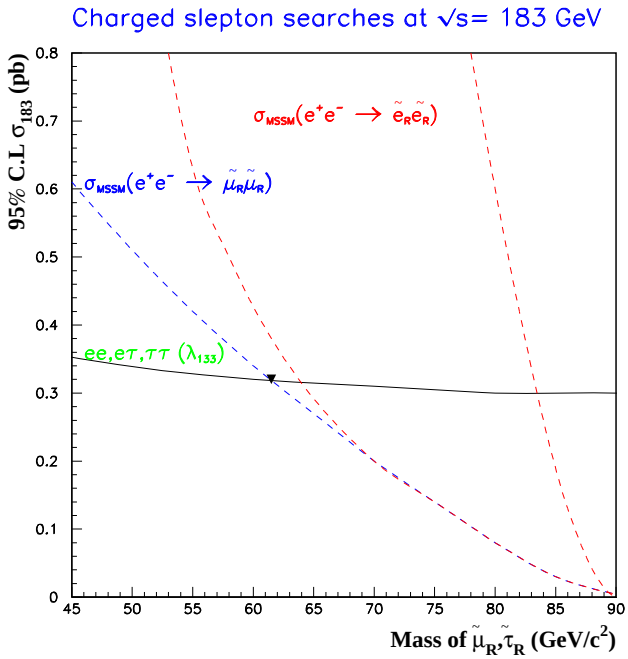

Figure 10: Slepton direct decay with λ coupling: the full line shows the limit on the $\widetilde{ll}$ cross section as a function of the slepton mass. The lower dashed curve gives the MSSM cross section for $\tilde{\mu}\tilde{\mu}$, $\tilde{\tau}\tilde{\tau}$ production. The other 2 dashed curves show the bounds of the $\tilde{e}\tilde{e}$ cross section since it depends on neutralino mass.

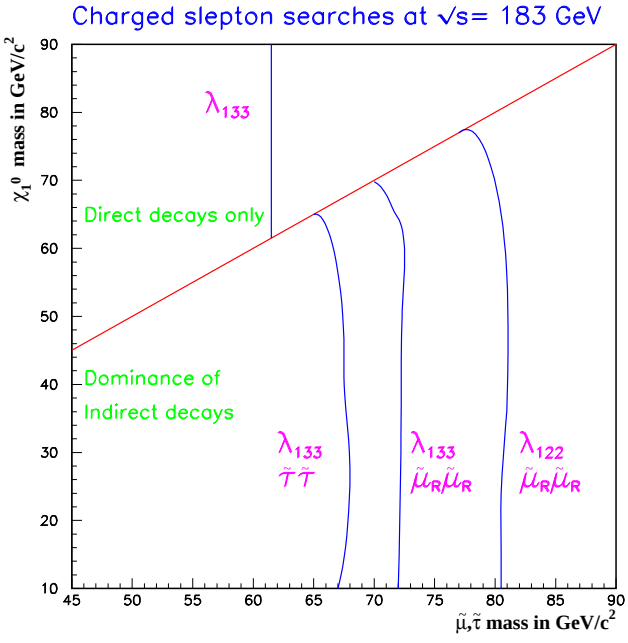

Figure 11: Slepton search with λ coupling: exclusion domain in $m_{\tilde{\chi}^0}$ versus $m_{\tilde{l}}$ for the $\tilde{l}$ pair production cross section; the diagonal line separates the plot in 2 regions: in the upper part, only the direct decay is allowed; in the lower part, the indirect decay is dominant, so the exclusion limit depends also on the neutralino mass. The limit is given by the direct decay.

4 $\not{R}_p$ decays with a dominant λ' coupling

There are 27 allowed λ'_{ijk} terms i.e. all combinations of i, j and k from 1 to 3. The simplest (and most conservative) assumption that one can make, is that one R-parity violating coupling is dominant. In table 12 we report the experimental limits from virtual exchange of R-Parity violating sparticles under this assumption [8].

ijk	$\lambda'_{ijk} \leq$	ijk	$\lambda'_{ijk} \leq$	ijk	$\lambda'_{ijk} \leq$
$\lambda'_{eud} - \lambda'_{\nu_e dd}(111)$	410^{-4}	$\lambda'_{\mu ud} - \lambda'_{\nu_\mu dd}(211)$	0.09	$\lambda'_{\tau ud} - \lambda'_{\nu_\tau dd}(311)$	0.10
$\lambda'_{eus} - \lambda'_{\nu_e ds}(112)$	0.02	$\lambda'_{\mu us} - \lambda'_{\nu_\mu ds}(212)$	0.09	$\lambda'_{\tau us} - \lambda'_{\nu_\tau ds}(312)$	0.10
$\lambda'_{ecd} - \lambda'_{\nu_e sd}(121)$	0.04	$\lambda'_{\mu cd} - \lambda'_{\nu_\mu sd}(221)$	0.18	$\lambda'_{\tau cd} - \lambda'_{\tau cd}(321)$	0.20
$\lambda'_{ecs} - \lambda'_{\nu_e ss}(122)$	0.02	$\lambda'_{\mu cs} - \lambda'_{\nu_\mu ss}(222)$	0.18	$\lambda'_{\tau cs} - \lambda'_{\nu_\tau ss}(322)$	0.20
$\lambda'_{eub} - \lambda'_{\nu_e db}(113)$	0.02	$\lambda'_{\mu ub} - \lambda'_{\nu_\mu db}(213)$	0.09	$\lambda'_{\tau ub} - \lambda'_{\nu_\tau db}(313)$	0.10
$\lambda'_{etd} - \lambda'_{\nu_e bd}(131)$	0.04	$\lambda'_{\mu td} - \lambda'_{\nu_\mu bd}(231)$	0.22	$\lambda'_{\tau td} - \lambda'_{\nu_\tau bd}(331)$	0.48
$\lambda'_{ecb} - \lambda'_{\nu_e sb}(123)$	0.2	$\lambda'_{\mu cb} - \lambda'_{\nu_\mu sb}(223)$	0.18	$\lambda'_{\tau cb} - \lambda'_{\nu_\tau sb}(323)$	0.20
$\lambda'_{ets} - \lambda'_{\nu_e bs}(132)$	0.34	$\lambda'_{\mu ts} - \lambda'_{\nu_\mu bs}(232)$	0.36	$\lambda'_{\tau ts} - \lambda'_{\nu_\tau bs}(332)$	0.48
$\lambda'_{etb} - \lambda'_{\nu_e bb}(133)$	0.0007	$\lambda'_{\mu tb} - \lambda'_{\nu_\mu bb}(233)$	0.36	$\lambda'_{\tau tb} - \lambda'_{\nu_\tau bb}(333)$	0.48

Table 12: Limits [10] on the $\not{R}_p$ couplings λ' in units of $(m_{\tilde{f}}/100\text{GeVcc})$, where $m_{\tilde{f}}$ is the appropriate sfermion mass.

The chargino/neutralino analysis described below is dedicated to λ'_{111}, λ'_{121}, λ'_{112}, λ'_{122}; i.e. the lepton (slepton) is e or ν_e ($\tilde{e}$ or $\tilde{\nu}_e$) and quarks (squarks) are u, d, c, s ($\tilde{u}, \tilde{d}, \tilde{c}, \tilde{s}$). As the top quark is too heavy, λ'_{133}, λ'_{132} and λ'_{131} couplings will lead to a unique final state with the production of one or two b quarks. The analysis of these couplings as well as λ'_{113} and λ'_{123} can be performed using b quark tagging techniques, and can give better sensitivity, therefore the limits obtained here can be considered conservative for all λ'_{1jk} couplings.

The different final states of the processes $e^+e^- \to \tilde{\chi}^0_1\tilde{\chi}^0_1$, $\tilde{\chi}^0_1\tilde{\chi}^0_2$, and $\tilde{\chi}^+_1\tilde{\chi}^-_1$, with $\not{R}_p$ decays are reported in table 13. Final states with jets and missing energy as well as final states with jets and one or more leptons (with or without missing energy) are possible.

The sneutrino direct decay analysis on the other hand, relies on the quark flavour since a sneutrino decaying through λ'_{333} to a pair of b's is considered as a possible interpretation of small remnant deviations in b asymmetries [23]. In this paper, the tau sneutrino $\not{R}_p$ decays to $d\bar{d}$ through $\lambda'_{\nu_\tau dd}(311)$, to $d\bar{b}$ quarks through $\lambda'_{\nu_\tau db}(313)$ and to $b\bar{b}$ through $\lambda'_{\nu_\tau bb}(333)$, are studied. The $\tilde{\tau}$ production and subsequent decay through $\lambda'(311)$ is also studied. The indirect decays will give a signal similar to the chargino/neutralino analysis with extra missing energy.

Finally, among the squarks the third generation has the highest probability to be the first accessible to an e^+e^- collider due to mixing and the strongest influence of Yukawa couplings. Furthermore, among the squark $\not{R}_p$ decays the stop has the particularity of having a dominant $\not{R}_p$ decay for a large domain of λ' values. This can be explained as follows: the expression of the width of the stop decaying directly[5] into ld (where ld can

[5]note that, with the $\lambda'_{ijk}L_iQ_j\bar{D}_k$ term of the $\not{R}_p$ superpotential, only the $\tilde{t}_L$ couples to leptons and down-type quarks. The mass eigenstate $\tilde{t}_1$ of the stop is defined as: $\tilde{t}_1 = \tilde{t}_L cos\theta_t + \tilde{t}_R sin\theta_t$

Signature	Channel(s)
4 jets ($\not\!\!E$)	$\tilde{\chi}_1^0\tilde{\chi}_1^0$ - $\tilde{\chi}_1^0\tilde{\chi}_2^0$ (D,I) - $\tilde{\chi}_1^+\tilde{\chi}_1^-$ (D)
6 jets ($\not\!\!E$)	$\tilde{\chi}_1^0\tilde{\chi}_2^0$ (I)
8 jets ($\not\!\!E$)	$\tilde{\chi}_1^+\tilde{\chi}_1^-$ (I)
1 lepton 4 jets ($\not\!\!E$)	$\tilde{\chi}_1^0\tilde{\chi}_1^0$ - $\tilde{\chi}_1^0\tilde{\chi}_2^0$ (D,I) - $\tilde{\chi}_1^+\tilde{\chi}_1^-$ (D)
1 lepton 6 jets ($\not\!\!E$)	$\tilde{\chi}_1^0\tilde{\chi}_2^0$ (I) - $\tilde{\chi}_1^+\tilde{\chi}_1^-$ (I)
1 lepton 8 jets ($\not\!\!E$)	$\tilde{\chi}_1^+\tilde{\chi}_1^-$ (I)
2 leptons 4 jets	$\tilde{\chi}_1^0\tilde{\chi}_1^0$ - $\tilde{\chi}_1^0\tilde{\chi}_2^0$ (D) - $\tilde{\chi}_1^+\tilde{\chi}_1^-$ (I)
2 leptons 4 jets ($\not\!\!E$)	$\tilde{\chi}_1^0\tilde{\chi}_2^0$ (I) - $\tilde{\chi}_1^+\tilde{\chi}_1^-$ (D)
2 leptons 6 jets	$\tilde{\chi}_1^0\tilde{\chi}_2^0$ (I)
2 leptons 6 jets ($\not\!\!E$)	$\tilde{\chi}_1^+\tilde{\chi}_1^-$ (I)
2 leptons 8 jets	$\tilde{\chi}_1^+\tilde{\chi}_1^-$ (I)
3 leptons 4 jets ($\not\!\!E$)	$\tilde{\chi}_1^0\tilde{\chi}_2^0$ (I) - $\tilde{\chi}_1^+\tilde{\chi}_1^-$ (I)
3 leptons 6 jets ($\not\!\!E$)	$\tilde{\chi}_1^+\tilde{\chi}_1^-$ (I)
4 leptons 4 jets	$\tilde{\chi}_1^0\tilde{\chi}_2^0$ (I)
4 leptons 4 jets ($\not\!\!E$)	$\tilde{\chi}_1^+\tilde{\chi}_1^-$ (I)

Table 13: Final states in neutralino and chargino pair production when a λ' coupling is dominant; D (I) means direct (indirect) decay of $\tilde{\chi}_1^+$ or $\tilde{\chi}_2^0$.

be ed, μd or τb) is given by [24]:

$$\Gamma(\tilde{t}_1 \to lq) = \frac{\lambda'^2}{16\pi} cos^2\theta_t m_{\tilde{t}_1} \tag{3}$$

where θ_t is the stop mixing angle [25]. This expression may be compared to the width of the decay into $\tilde{\chi}_1^0$, given by [26]:

$$\Gamma(\tilde{t}_1 \to c\tilde{\chi}_1^0) = (0.3-3)\times 10^{-10} m_{\tilde{t}_1} \left[1 - \frac{m^2_{\tilde{\chi}_1^0}}{m^2_{\tilde{t}_1}}\right]^2 \tag{4}$$

The corresponding decay time ($\geq 10^{-20}$ sec) is far longer than the strong-interaction time scale of the order of 1 fm (i.e. $O(10^{-23})$ sec), so that a produced $\tilde{t}_1$ hadronizes into a stop hadron before it decays. The stop hadronization also occurs before decaying in the $\not\!R_p$ mode, for values of the λ' coupling lower than $O(10^{-1})$. As the relevant current HERA limit on λ' [27] for stop masses accessible to LEP2 already excludes λ'_{131} above $O(10^{-2})$ we will take the attitude of considering that the stop always hadronizes before decaying via $\not\!R_p$ couplings.

Equating the width $\Gamma(\tilde{t}_1 \to ld) = \Gamma(\tilde{t}_1 \to c\tilde{\chi}_1^o)$ for $\theta_t = 0$ i.e. pure left stop, gives:

$$\lambda'^2 = 16\pi(0.3-3)\times 10^{-10}[1 - \frac{m^2_{\tilde{\chi}_1^o}}{m^2_{\tilde{t}_1}}]^2 \tag{5}$$

Thus one can estimate the accessible range of the λ' couplings involved in the direct stop decay into ld.

For conservative values in the theoretical uncertainty [26] of $\Gamma(\tilde{t}_1 \rightarrow c\tilde{\chi}_1^o)$, i.e. 3×10^{-10} and no suppression by phase space, one obtains the minimum value of λ', $\lambda'_{min} = 1.2 \times 10^{-4}$ above which direct decays dominate. For small mass differences between $\tilde{\chi}_1^0$ and the stop, the suppression due to phase space gives a λ'_{min} closer to 10^{-5}.

For λ' below λ'_{min}, we expect that the stop decays first into charm and $\tilde{\chi}_1^0$ and then the $\tilde{\chi}_1^0$ may decay via $\not{R}_p$ giving more complicated topologies than 2 l, 2 $jets$ and no missing energy. By restricting ourselves to the 2 l, 2 $jets$ and no missing energy topology, we do not explore coupling values below λ'_{min}. This very conservative value of the coupling will be taken as our limit if no evidence for this topology is found in our data.

In summary, while the studies in this section for the charginos/neutralinos can be considered exhaustive and conservative, for the sneutrinos, charged sleptons and squarks, they have to be complemented by the indirect decays, not studied yet.

4.1 Neutralinos and charginos decaying through λ'

The production of charginos and neutralinos for a large region of the μ, M_2 plane and for 4 characteristic combinations of $tan\beta$ and m_0: (1.5, 90), (1.5, 300), (30, 90) and (30, 300) has been studied.

Out of the λ' couplings considered in this part (λ'_{111}, λ'_{121}, λ'_{112}, λ'_{122}) the neutralinos produced by pairs can decay into three different topologies:

- 4 jets + 2 electrons;
- 4 jets + 2 neutrinos (i.e. missing energy);
- the mixed case where with the same λ', one neutralino decays into 1 electron and 2 jets and the other into 1 neutrino and 2 jets.

The case of 4 $jets$ + 2e in the final state is examined in the section 4.1.1. The case of 4 $jets$ + $\not{E}$ in the final state is dominated by high background, therefore although it has been studied using a dedicated analysis, it is not used for deriving the exclusion domain. The region in the MSSM parameter space, where this decay dominates, is covered either by the results of chargino analysis which gives a better efficiency, or by the results of LEP1 as it is reported in the section 4.1.3. No search for the mixed case has been performed since the rest of the analyses were sufficient to reach the kinematical limit.

Concerning the chargino pair production, the regions where either the direct chargino decay is dominant or the charginos are lighter than 45 GeV/c^2, are covered by LEP1 results on total and partial decay widths of the Z boson (see section 4.1.3). For the indirect decays $\widetilde{\chi}^{\pm} \rightarrow \widetilde{\chi}_1^0 \mathrm{W}^*$ and when the chargino is heavier than 45 GeV/c^2, the analysis performed for $\widetilde{\chi}_1^0\widetilde{\chi}_1^0$ pair production leading to 2e + 4jets in the final state is used for neutralino decays to e+ 2jets, and a dedicated analysis is performed (see section 4.1.2) when the neutralino decays into 1ν+ 2jets.

4.1.1 $\tilde{\chi}_1^0$ decay into e 2jets

The most spectacular signature is the direct decay of the lightest neutralino to an electron and two jets (i.e. $\tilde{\chi}_1^0 \rightarrow e^- c\bar{d}$ or $\tilde{\chi}_1^0 \rightarrow e^+ \bar{c}d$ for λ'_{121}) . The presence of an electron in the final state provides efficient selection criteria.

Events are preselected if they verify the following requirements:

- the total event multiplicity must be greater or equal to 15, and the charged multiplicity greater or equal to 10;

- at least one electron must be identified.

These cuts remove the low multiplicity background events, such as bhabha and most of $\gamma\gamma$ events.

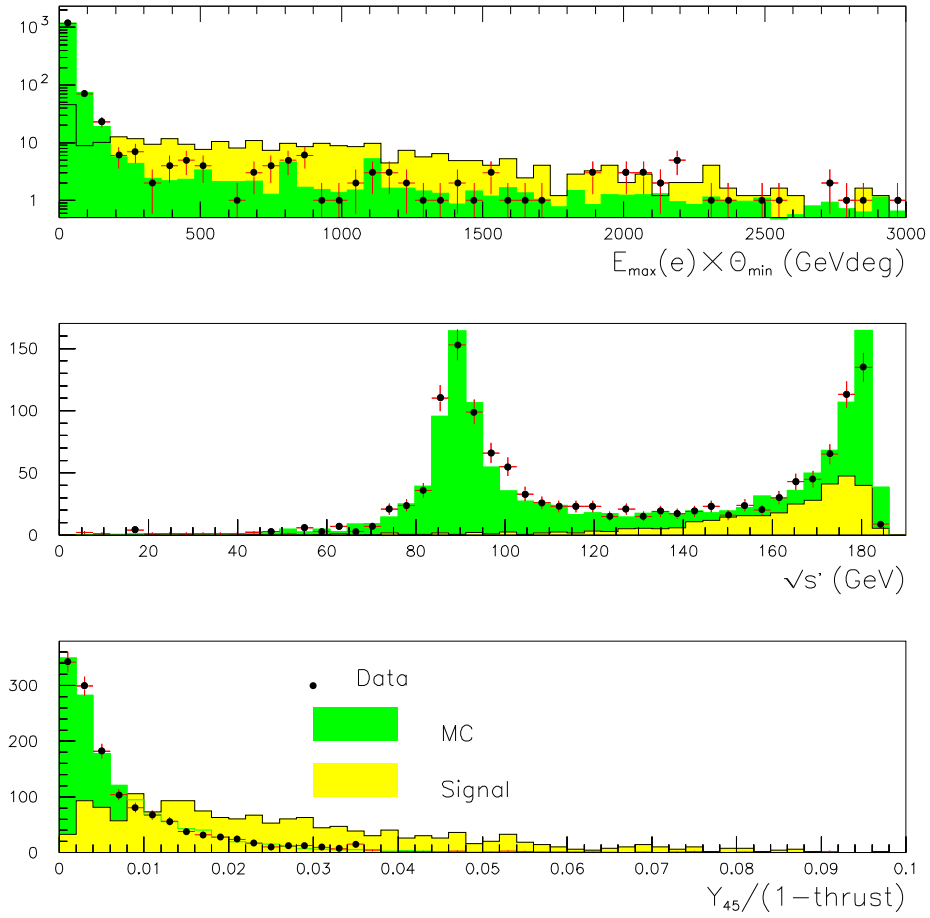

Figure 12: Neutralino into $e+2$ jets (λ' coupling) analysis: distributions of $E_{max}(e)\times\theta_{min}$, $\sqrt{s\prime}$, and $Y_{45}/(1-\text{thrust})$ for data (dots), expected SM background (dark grey or green in colour) and $\widetilde{\chi}^0_1\widetilde{\chi}^0_1$ signal (light grey or yellow in colour) events after the preselection.

After this event pre-selection, the analysis proceeds as follows:

- a lower cut of 190 GeV deg is applied on the value of $E_{max}(e)\times\theta_{min}$ where $E_{max}(e)$ is the energy of the most energetic electron (in case of more than one electron identified in the event) and θ_{min} is the minimum angle (in degrees) between this electron and the nearest charged particle;
- the energy available in the e^+e^- collision after initial state radiation ($\sqrt{s\prime}$) must be greater than 155 GeV;
- the ratio $Y_{45}/(1-\text{thrust})$ where Y_{45} is the value of the DURHAM distance at which the event topology flips from 5 to 4 jets, must be greater than 0.01;
- the missing momentum of the event must be lower than 40 GeV/c.

These requirements remove all remaining $\gamma\gamma$ background and reduce significantly the contribution of Zγ, Z $\to q\bar{q}$ events and the four fermion final state (ZZ, $\mathrm{W^+W^-}$) events.

The distributions of variables used in the analysis are shown in figure 12; the number of remaining real and background events after these cuts are reported in table 14. 3 events remain in the data, with 3.3 expected SM background (2.33 from Zγ, Z $\to q\bar{q}$, 0.98 from ZZ, W^+W^-).

Cuts	Data	Total background	Efficiency (%)
Total multiplicity$\geq$15 Charged multiplicity$\geq$10 At least one electron	1366	1377	75
$E_{max}(e)\times\theta_{min} \geq$ 190 GeV deg.	102	96.8	62
$\sqrt{s\prime} \geq$155 GeV	19	21.0	46
Y_{45}/(1$-$thrust) $\geq$0.01	5	3.7	38
$P_{miss} \leq$ 40 GeV/c	3	3.3	35
Lower limit for exclusion of signal at 95% CL : $N_{95} = 5.3$			

Table 14: $\tilde{\chi}_1^0 \to e^-$2jets analysis: applied criteria, selected data, remaining background and typical efficiency obtained.

This analysis was also applied to $\tilde{\chi}_1^0\tilde{\chi}_2^0$, $\tilde{\chi}_1^0\tilde{\chi}_3^0$ and $\tilde{\chi}_1^+\tilde{\chi}_1^-$ (for the indirect decay of $\tilde{\chi}_2^0$, $\tilde{\chi}_3^0$ and $\tilde{\chi}_1^\pm$, in case of $\tilde{\chi}_1^0$ decaying into e + 2jets). The efficiencies obtained are between 25 and 40 %.

4.1.2 Indirect decay of charginos with mass > 45 GeV/c^2

The analysis described in this section is sensitive to both hadronic and leptonic decay of the W, coming from the indirect decay of charginos (figure 3), when the neutralinos decay into a neutrino and 2 jets.

Events are pre-selected if they have a charged multiplicity greater than 8, if the ratio between the total energy from charged particles and the missing energy is lower than 2, and if the missing transverse momentum is greater than 5 GeV/c. These pre-selection criteria remove bhabha and most of $\gamma\gamma$ events.

The selection proceeds as follows:

- the value of $Y_{34} \times Y_{45}$, where Y_{34} (Y_{45}) is the value of the DURHAM distance at which the event topology flips from 5 to 4 jets (from 4 to 3), must be greater than 10^{-5} which removes 90 % of remaining Zγ background.
- the absolute value of the cosinus of the missing momentum polar angle must be lower than 0.8;
- the ratio between the visible mass and the missing energy must be in the [0.4, 1.6] range;
- the acolinearity must be lower than 0.6 rad;
- the missing momentum must be greater then 10 GeV/c.

The remaining background, after this selection, is composed of W^+W^- (40 %) and Zγ (60 %). The effect of the selection criteria on data and background events are summarized in table 15, and the distributions, after the pre-selection, of variables used in the selection procedure are shown in figure 13; the agreement between data (dots) and

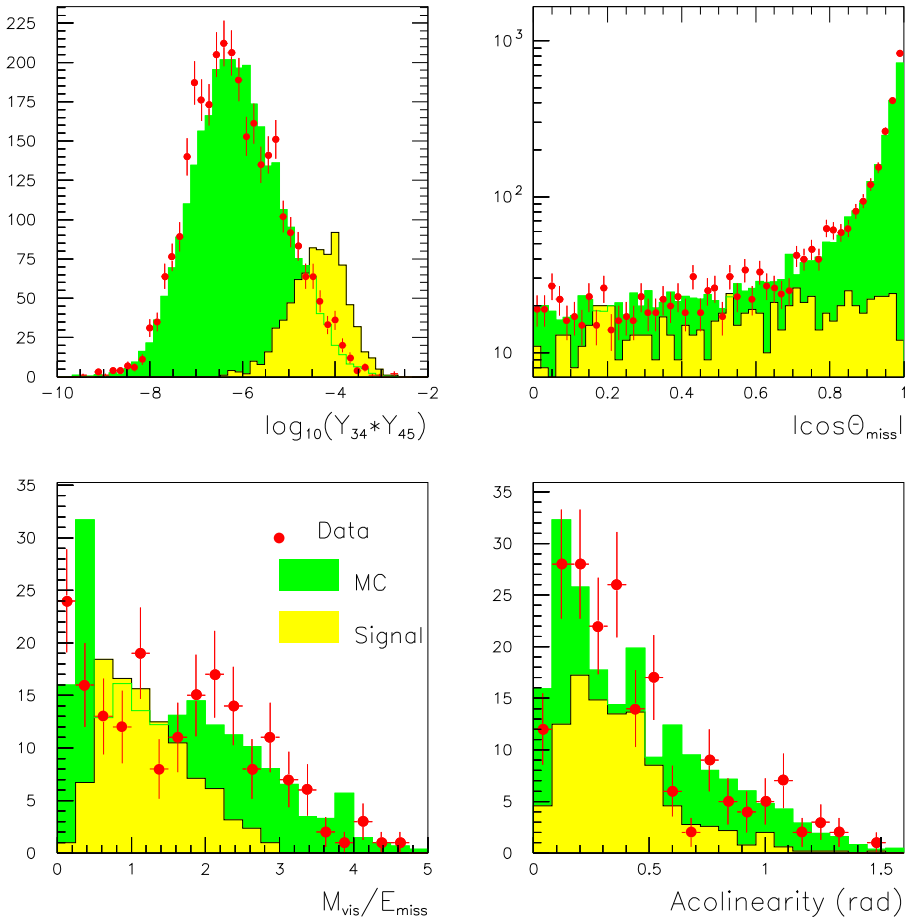

Figure 13: Chargino indirect decay (λ' coupling) analysis: distributions of $\log_{10}(Y_{34} * Y_{45})$, $|cos(\theta_{miss})|$, M_{vis}/E_{miss} and acolinearity for data (dots), expected SM background (dark grey or green in colour) and $\widetilde{\chi}_1^+\widetilde{\chi}_1^-$ signal (light grey or yellow in colour) events. The distributions are those obtained after the preselection criteria.

MC (dark grey) is fairly good. The chargino pair production signal (light grey, yellow in colour), is generated with a mass $m_{\chi}^{\pm}$ =50 GeV/c^2.

The results are interpreted in terms of the MSSM in section 4.4 and shown in figure 17.

4.1.3 LEP1 exclusion regions

The LEP lineshape data and the left-right asymmetry measured at SLD give an almost model independant upper limit of 6.3 MeV on the decay width of the Z into new particles at 95% confidence level [28]. This corresponds to an upper limit of 150 pb on the cross section, in the s-channel, for any "new" process. This limit can be used to exclude MSSM parameter regions where the cross section of neutralino/chargino pair production is higher than this value. The corresponding excluded area in μ, M_2 plane for 2 values of $tan\beta$ and 2 values of m_0 is shown in figure 17 (light grey area, yellow in colour).

Cuts	Data	Total background	Efficiency (%)
Charged multiplicity > 8 $E_{charged}/E_{miss} \leq 2$ missing $p_t \geq 5$ GeV/c	3135	3015	80
$Y_{34} * Y_{45} \geq 10^{-5}$	436	411	68
$\|cos(\theta_{miss})\| < 0.8$	194	199	51
$0.4 \leq M_{vis.}/E_{miss.} \leq 1.6$	62	70.4	36
Acolinearity$\leq$0.6	34	38.9	30
$P_{miss} \geq 10$ GeV/c	27	30.3	27
Lower limit for exclusion of signal at 95% CL: $N_{95} = 10.3$			

Table 15: Heavy chargino indirect decay analysis: applied criteria, selected data, remaining background and typical efficiency obtained.

4.2 Sneutrinos and charged sleptons decaying through λ'

Contrary to studies of previous sections, in this search the events from runs at center of mass energies of 161 GeV ($\mathcal{L}$= 9.7 pb^{-1}) and 172 GeV ($\mathcal{L}$= 10.0 pb^{-1}) are also used. Hadronic events are selected by requiring at least 12 charged particles, a total of charged energy above $0.30\sqrt{s}$ and a total energy exceeding $0.40\sqrt{s}$. In order to reduce the radiative $q\bar{q}\gamma$ background the maximum photon energy E_γ^{max} or the "unseen" calculated photon energy (E_γ^{cal})[6] is required to be less than 35 GeV.

The DURHAM algorithm is used to reconstruct jets. A y_{cut} value of 0.008 is applied. If the number of jets is less than four then the event is rejected otherwise it is forced to be a four jet event.

- **The $\lambda'_{\nu_\tau dd}(311)$, $\lambda'_{\nu_\tau db}(313)$, $\lambda'_{\nu_\tau bb}(333)$, $\lambda'_{\tau ud}(311)$ search**

The same selection criteria are applied for all the λ'_{3jk} terms while b-tagging is applied only for the $\lambda'_{\nu_\tau db}(313)$ and $\lambda'_{\nu_\tau bb}(333)$ searches. The selection criteria are described below.

- All four jet events are required to satisfy energy and momentum conservation by applying a kinematical (4C) fit [29]. Then the χ^2_{4C} is required to be less than 25 to reduce the badly reconstructed or radiative events.
- The remaining radiative $q\bar{q}\gamma$ background can be further reduced by requiring a jet to have at least 2 charged particles, an electromagnetic energy less than $0.8E_{jet}$ and a mass m_{jet} greater than 1 GeV/c^2.
- The QCD background is further reduced by applying a cut on the following four jet event shape variables [30]: the product $\alpha_{min} \times E_{min}$, where α_{min} is the minimum angle between two jets, E_{min} the lowest energy of the jets and $\beta_{min} \times \frac{E_{max}}{E_{min}}$, where β_{min} is the minimum angle between the highest energetic jet and the three others. The $\alpha_{min} \times E_{min}$ is required to be greater than $15 + 0.5 \times \beta_{min} \times \frac{E_{max}}{E_{min}}$.
- The 4-parton matrix element for $e^+e^- \to q\bar{q}gg$ is calculated as defined in [31]. A "QCD-probability" P_{QCD} is formed, taking as inputs the jet four vectors, and only events with low P_{QCD} are retained.

[6] E_γ^{cal} is the undetected missing photon energy and is computed from energy and momentum conservation, assuming a photon collinear to the beam axis.

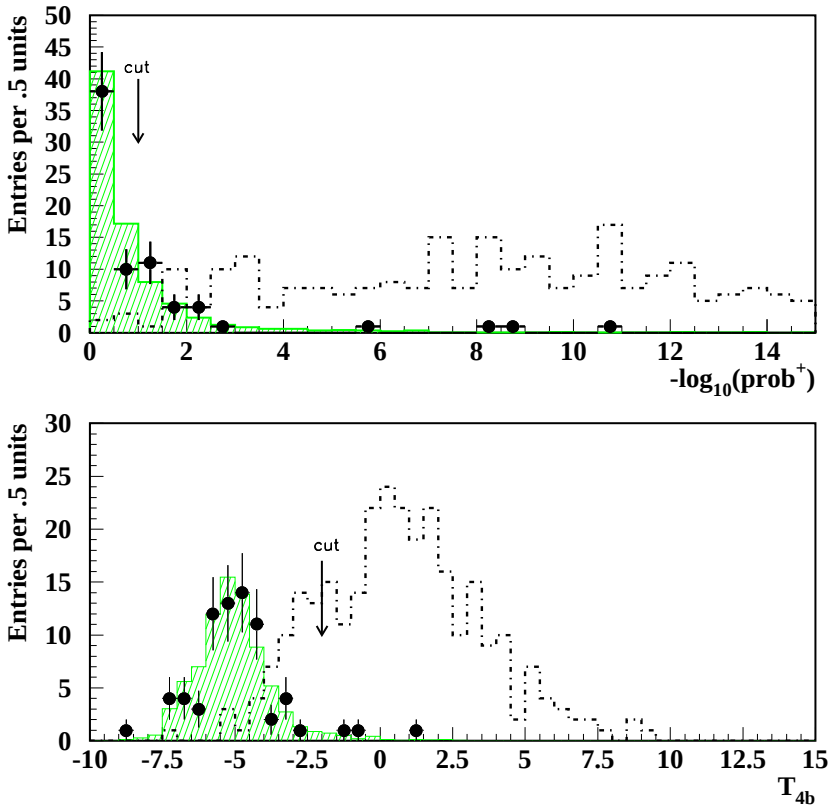

Figure 14: Sneutrino searches with a dominant λ' coupling: distributions of b-tagging variables after the four jet selection for real data (black dots), SM (QCD, W^+W^- and ZZ) background (hatched histogram) and a $\tilde{\nu}_\tau$ signal with mass equal to 45 GeV/c^2 (dotted histogram). The arrows show the applied cuts.

- The mass reconstruction is done by applying a kinematical fit with five constraints (5C) [29], where the additional fifth constraint requires the production of two equal mass objects. For a 45 GeV/c^2 sneutrino a resolution of 1.42 GeV/c^2 is obtained.

The event and jet tagging is done by using the AABTAG algorithm [32]. This algorithm combines information from impact parameters and rapidities of the tracks, the masses from the secondary vertices and the fraction of the energy taken by B-hadrons in the jets. An event tagging variable T_{4b} as described in [32] is defined to distinguish four b-jet events from QCD and W$^+$W$^-$ event topologies. The distributions of the b-tagging variables, (event probability for positive impact parameters $-log_{10}(prob^+)$ and the tagging variable T_{4b}), for data, SM background and the $\tilde{\nu_\tau} \to bb$ signal at $\sqrt{s}$ =172 GeV are shown in figure 14.

For the $\lambda'_{\nu_\tau db}(313)$ search (i.e $2b$ quarks in the event) the event probability $-log_{10}(prob^+)$ must be greater than 1, while for the $\lambda'_{\nu_\tau bb}(333)$ search (i.e $4b$ quarks in the event) the additional requirement of $T_{4b} >$ -2 is applied.

Results are summarized in table 16. The distributions of data and SM background processes before b-tagging is shown in figure 15. The bulk of the events in the non-b case

Selection criteria	data			$q\bar{q}\gamma$			W^+W^-, ZZ			eff.(%), $\lambda'_{\nu_\tau db}$ $m_{\tilde{\nu}_\tau}$=55 GeV/c^2
	E_{CM} GeV									
	161	172	183	161	172	183	161	172	183	
Four jets $y^D_{cut} > 0.008$	53	72	390	40	26	100	14	52	301	88
$\chi^2_{4C} < 25$	47	64	348	33	22	87	13	48	285	85
ISR and QCD	15	35	235	9	8	37	10	38	236	48
$-log_{10}(prob^+) > 1$ for($\lambda'_{\nu_\tau db}$,$\lambda'_{\nu_\tau bb}$)	3	13	74	3	3	14	2	9	63	42
$T_{4b} > -2$ only for $\lambda'_{\nu_\tau bb}$	0	1	4	0.6	0.4	3	0.05	0.15	2	

Table 16: Data and SM background events at three center of mass energies (161, 172 and 183 GeV), compared to the signal efficiency for a $\tilde{\nu}_\tau$ (produced at center of mass energy of 172 GeV) with mass equal to 55 GeV/c^2.

is concentrated around the W mass as can be seen in figure 15.

For the $\not{R}_p$ terms $\lambda'_{\nu_\tau dd}(311)$, $\lambda'_{\nu_\tau db}(313)$ and $\lambda'_{\nu_\tau bb}(333)$ the efficiencies for different sneutrino masses are presented in table 17. In the last two rows the b-tagging algorithm is applied.

Finally, the direct decay of $\tilde{\tau} \to ud$ via the $\lambda'_{\tau ud}(311)$ coupling was considered. The analysis used is the same as for the sneutrino decays via $\lambda'_{\nu_\tau dd}(311)$ term with also the same detection efficiency.

The interpretation of results is presented in section 4.4. Figure 18 shows the number of expected events derived for each type of λ' coupling studied, as a function of the $\tilde{\nu_\tau}$, $\tilde{\tau}$ mass. The number of expected events that can be excluded at 95% confidence level is obtained by counting the number of events in data and SM background with dijet masses from 54 to 76 GeV/c^2, using a 2 GeV/c^2 bin and having a window of $\pm$ 4 GeV/c^2 in each mass. Data and SM background events are taken from figure 15.

$\not{R}_p$ terms	$m_{\tilde{\nu}_\tau}$														
	55 GeV/c^2 eff.(%)			60 GeV/c^2 eff.(%)			65 GeV/c^2 eff.(%)			70 GeV/c^2 eff.(%)			75 GeV/c^2 eff.(%)		
	E_{CM} GeV														
	161	172	183	161	172	183	161	172	183	161	172	183	161	172	183
$\lambda'_{\nu_\tau dd}$	44	44	47	49	47	49	50	49	52	52	51	50	53	49	51
$\lambda'_{\nu_\tau db}$	44	42	43	44	46	45	48	45	49	49	50	48	50	50	50
$\lambda'_{\nu_\tau bb}$	43	44	45	45	50	49	50	48	53	55	53	55	55	55	58

Table 17: The efficiency as a function of the $\tilde{\nu}_\tau$ mass after all cuts at center of mass energy of 161, 172, and 183 GeV.

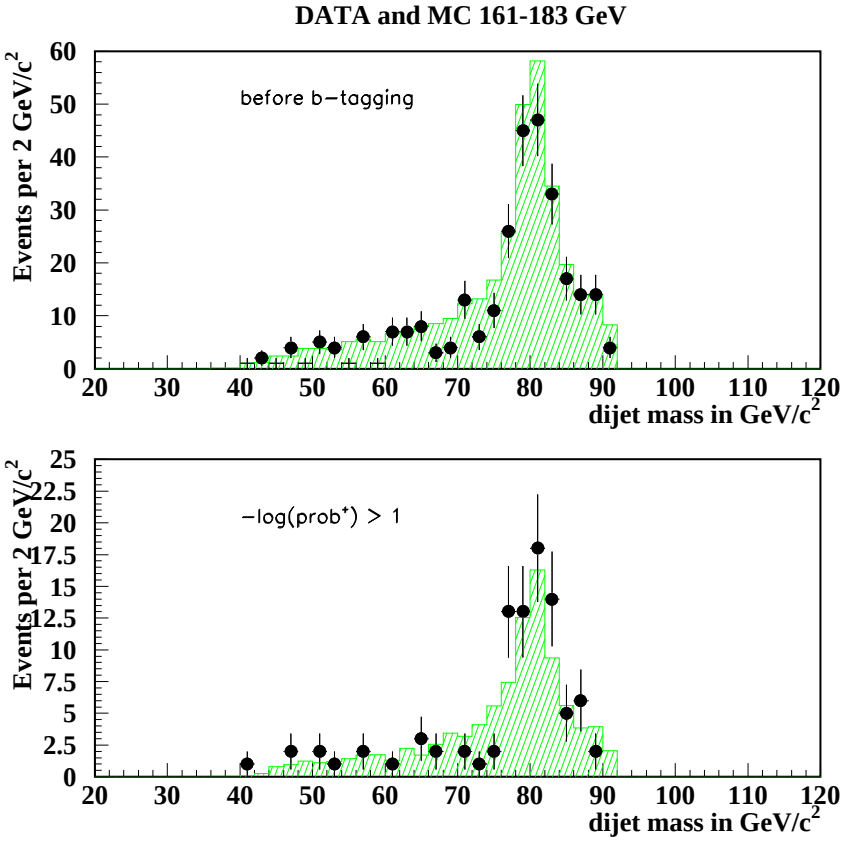

Figure 15: Sneutrino searches with a dominant λ' coupling: distribution of dijet masses for data (black dots), SM (QCD, W^+W^- and ZZ) background (hatched histogram) before and after $-log_{10}(prob^+)$ >1 cut is applied for the center-of-mass energies of 161-183 GeV. Those two plots are used for the mass limit calculation.

4.3 Stop decays to leptons and jets

In this section we will concentrate on cases where the λ'_{131} or λ'_{231} couplings are dominant. In this case, we have either the decay $\tilde{t}_1 \longrightarrow ed$, for the dominant coupling λ'_{131}, leading to the signature $2e$, 2 $jets$ and no missing energy or the decay $\tilde{t}_1 \longrightarrow \mu d$, for the dominant coupling λ'_{231}, leading to the signature 2μ, 2 $jets$ and no missing energy. The lightest stop $\tilde{t}_1$ is produced in pairs [25]. In both cases, λ'_{131} and λ'_{231}, we have the signature $2\ l\ +\ 2\ jets$.

The stop and sbottom event generators used the program package GRACE [33] for the calculation of the matrix elements, and the program packages BASES and SPRING described in [34] for the phase space generation and event production. The differential cross section function is based on the calculation of [35] which includes initial state QED correction in the collinear approximation at the leading order as well as QCD corrections. The process of hadronization was carried out with JETSET 7.3 [12] (some more details on hadronization in [25], [36]). Stop signals were simulated at different masses and decay patterns at the two energies which then passed through full DELPHI simulation.

The selection used for the present analysis has been derived from the original analysis of the 1996 data designed for the search of the higgs boson in the hZ mode where 2 leptons

(μ μ or e e) and 2 jets are produced [37]. The selection has been modified by including an optimisation of some of the cuts and by performing a four constraint (4C) kinematical fit in view of reconstructing two equal mass objects, one object being reconstructed from one jet and one lepton. The four contraints of the kinematical fit includes conservation of the energy and momentum. Considering the combination of leptons L_i (jets J_j), with $i = 1, 2$ indicating respectively the most energetic lepton (jet) and the second most energetic lepton (jet), the lepton-jet invariant mass M_{LJ} is shown in figure 4.3 in the combination J_1, L_2 and J_2, L_1 (which minimizes the mass differences $M_{L_i J_j} - M_{L_k J_l}$), for the case where the leptons are muons i.e. in the case of $\tilde{t}_1 \to \mu d$ with a stop $\tilde{t}_1$ of 70 GeV/c^2 mass.

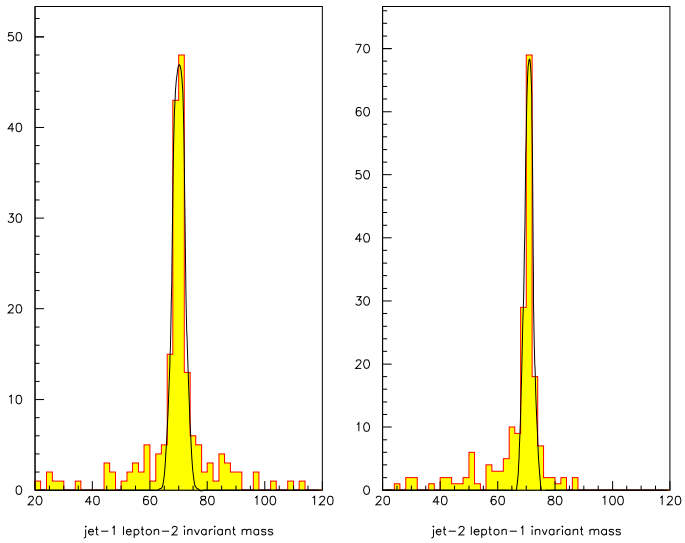

Figure 16: Stop searches with a dominant λ' coupling: lepton-jet invariant mass M_{LJ}. The combination of leptons L_i (jets J_j), with $i = 1, 2$ indicating respectively the most energetic lepton (jet) and the second most energetic lepton (jet), gives 4 invariant masses. The combination J_1, L_2 and J_2, L_1 which minimizes the mass differences $M_{L_i J_j} - M_{L_k J_l}$ is chosen.

The event selection proceeds as follows:

- hadronic events are selected by requiring at least 8 charged particles in the barrel acceptance and a total energy from charged particles above 16% of $\sqrt{s}$;
- among the charged particles, at least two fast charged particle with $p_1 > 8$ GeV/c and $p_2 > 16$ GeV/c with opposite charges are required; these are then considered as the two lepton candidates.
- the selection proceeds by requiring an isolation of 3^o and polar angles in the range of $[5^o, 175^o]$ for these lepton candidates, 2 or 3 jets in the event using a JADE-like jet algorithm;
- finally, making use of the information from the 4C kinematical fit, the following requirements are imposed:

  $\chi^2_{4C} < 20$ for the $\tilde{t}_1 \to ed$ case, $\chi^2_{4C} < 10$ for the $\tilde{t}_1 \to \mu d$ case;
  $\mid M_{J2L1} - M_{J1L2} \mid < 25$ GeV/c^2;
  M_{J2L1} and M_{J1L2} greater than 50 GeV/c^2.

The effects of these selections in the data as well as in simulated samples of background events, different from those used for the optimisation procedure, are shown in table 18 at $\sqrt{s} = 183$ GeV.

Channel	data	MC	$ff(\gamma)$	4-fermions	$\gamma\gamma$
$\tilde{t}_1 \to ed$	2	2.29 $\pm$ 0.44	1.02	0.95	0.31
$\tilde{t}_1 \to \mu d$	0	1.50 $\pm$ 0.20	1.15	0.35	0

Table 18: Effect of the selection the for λ'_{131} and λ'_{231} search.

The first candidate found in the data for the $\tilde{t}_1 \to ed$ channel has a total energy of 138.7 GeV. It contains two candidate leptons of momentum 16.2 GeV/c and 16.1 GeV/c respectively. The lepton-jet invariant masses are 59.7 GeV/c^2 and 75.1 GeV/c^2 respectively. The second candidate has a total energy of 149.6 GeV, two candidate leptons of momentum 57.4 GeV/c and 40.6 GeV/c and lepton-jet invariant masses of 63.0 GeV/c^2 and 83.4 GeV/c^2 respectively. Signal efficiencies are given in table 19 for stop masses of 60, 70, 80 and 90 GeV/c^2.

channel	60	70	80	90
$e\ d$	14.0 $\pm$ 2.6	17.7 $\pm$ 2.9	15.0 $\pm$ 2.6	17.2 $\pm$ 2.9
$\mu\ d$	21.64 $\pm$ 3.1	26.9 $\pm$ 3.5	23.5 $\pm$ 3.2	19.4 $\pm$ 2.8

Table 19: Signal efficiencies (in %) for the λ'_{131} and λ'_{231} search at $\sqrt{s} = 183$ GeV.

4.4 Interpretation of λ' dominant searches in terms of MSSM parameters

No deviation from Standard Model has been observed in the chargino/neutralino searches, therefore we can derive exclusion contours in the μ, M_2 plane. Four different planes were studied for different values of $tan\beta$ and m_0: $tan\beta = 1.5$ and $tan\beta = 30$, $m_0 = 90$ GeV/c^2 and $m_0 = 300$ GeV/c^2. The results are shown in figure 17 and are valid for λ'_{111}, λ'_{121}, λ'_{112} and λ'_{122} couplings.

For the sneutrinos, masses lower than 76 GeV/c^2, 72 GeV/c^2 and 60 GeV/c^2 are excluded at 95% confidence level for $\lambda'_{\nu_\tau bb}(333)$, $\lambda'_{\nu_\tau db}(313)$ and $\lambda'_{\nu_\tau dd}(311)$ violating terms respectively. The analysis for the sneutrino is also applied to the $\tilde{\tau}$ decay in case of $\lambda'_{\tau ud}(311)$ term, with the same detection efficiency as the one of $\lambda'_{\nu_\tau dd}(311)$ search. A stau mass lower than 71 GeV/c^2 is excluded at 95% confidence level. The results are shown in figure 18.

There is no evidence for a 2 l, 2 $jets$ and no missing energy topology in the data at $\sqrt{s} = 183$ GeV which can not be interpreted in terms of SM processes. No signal for stop decaying into ed or into μd has been found in the data. In consequence, limits on the stop mass at the 95 % confidence level can be derived for the ed channel and for the μd channel for a pure left stop i.e. a mixing angle equal to 0. The two stop decay channels have to

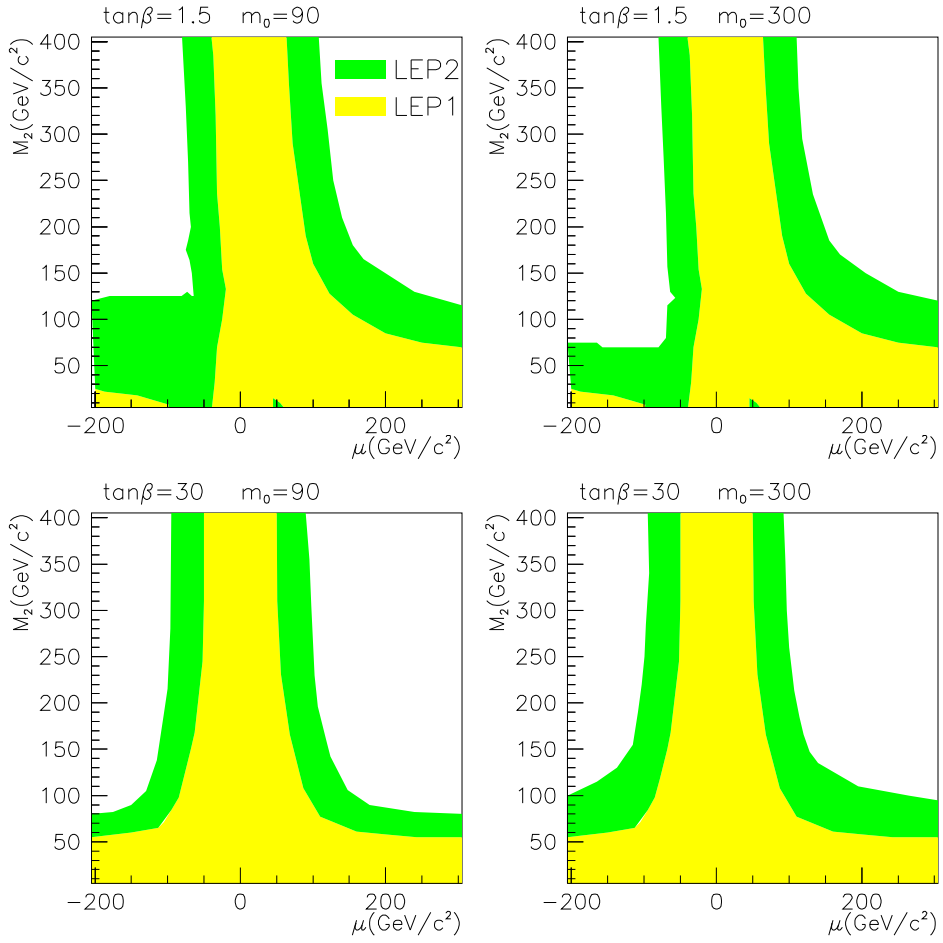

Figure 17: Neutralino and chargino searches with a dominant λ' coupling: regions in μ, M_2 parameter space excluded at 95 % C.L. for two values of tanβ and two values of m_0. The exclusion area obtained from LEP1 is shown in light grey and the corresponding area for the LEP2 ($E_{cm} = 183$ GeV) search is shown in dark grey. These exclusion regions are valid for λ'_{111}, λ'_{112}, λ'_{121}, λ'_{122} couplings.

be considered separately since they refer to two different $\not{R}_p$ couplings. For $\tilde{t}_1 \to ed$, a stop lighter than 73 GeV/c^2 is excluded at 95 % C.L., and for $\tilde{t}_1 \to \mu d$ a stop lighter than 81 GeV/c^2 is excluded at 95 % C.L

In the case of a zero stop mixing angle i.e. a pure left stop, λ'_{min} has been established conservatively to be equal to 1.1 10^{-4}, so that we have the boundaries λ'_{131} and $\lambda'_{231} < 1.1\ 10^{-4}$. The exclusion domain in the λ'_{131} and $m_{\tilde{t}_1}$ plane are shown in figure 19 and compared with other searches from HERA. While the range of accessible stop masses is modest when compared to the range of H1, λ'_{131} coupling values can be excluded down to the 10^{-5} level which are about 2 orders of magnitude below the H1 limits. Even lower coupling values can be explored when considering more complicated signatures than 2 l, 2 *jets* and no missing energy i.e. signature in which the stop first goes into charm and $\tilde{\chi}^0_1$ and then the $\tilde{\chi}^0_1$ decaying via the λ'_{131} $\not{R}_p$ coupling.

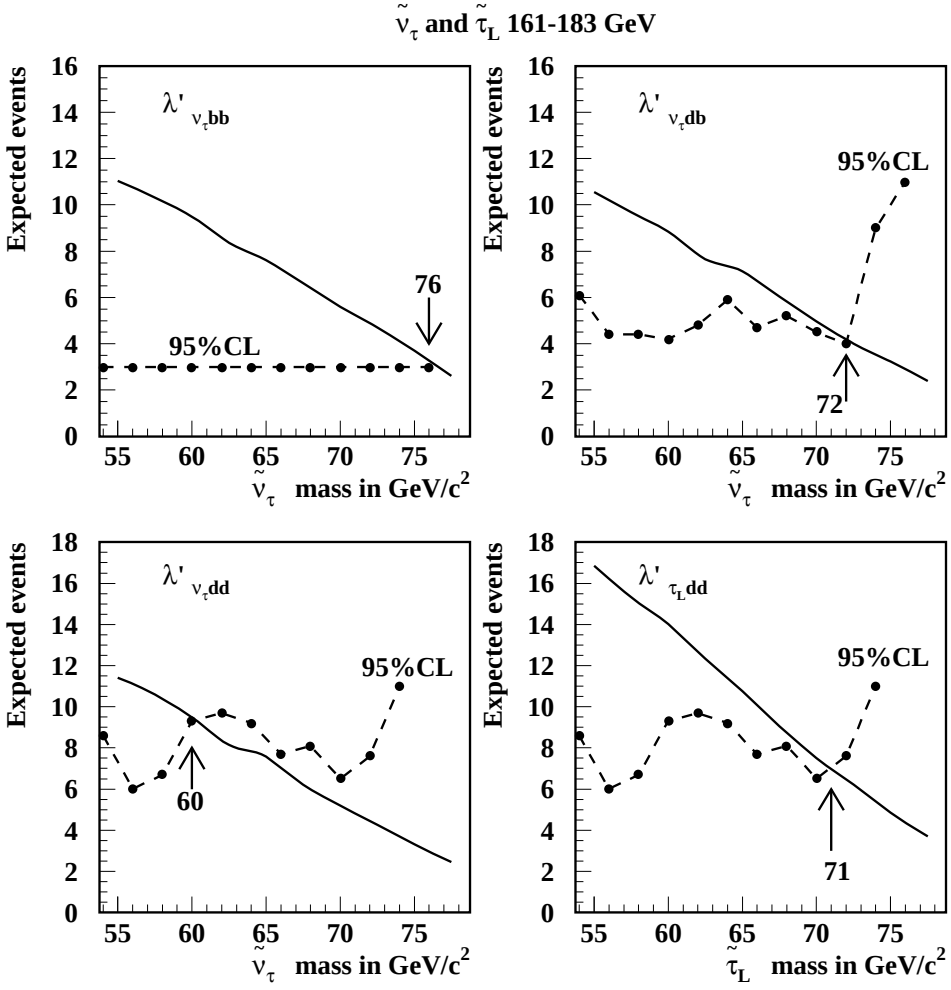

Figure 18: Sneutrino and stau searches with a dominant λ' coupling: expected events (dots connected with a dotted line) versus mass at 95% CL for the $\lambda'_{\nu_\tau dd}(311)$, $\lambda'_{\nu_\tau bb}(313)$, $\lambda'_{\nu_\tau bb}(333)$ and $\lambda'_{\tau ud}(311)$ terms. The solid line represents the number of expected events from the MSSM cross section taking into account the integrated luminosity and the efficiency at each center of mass energy.

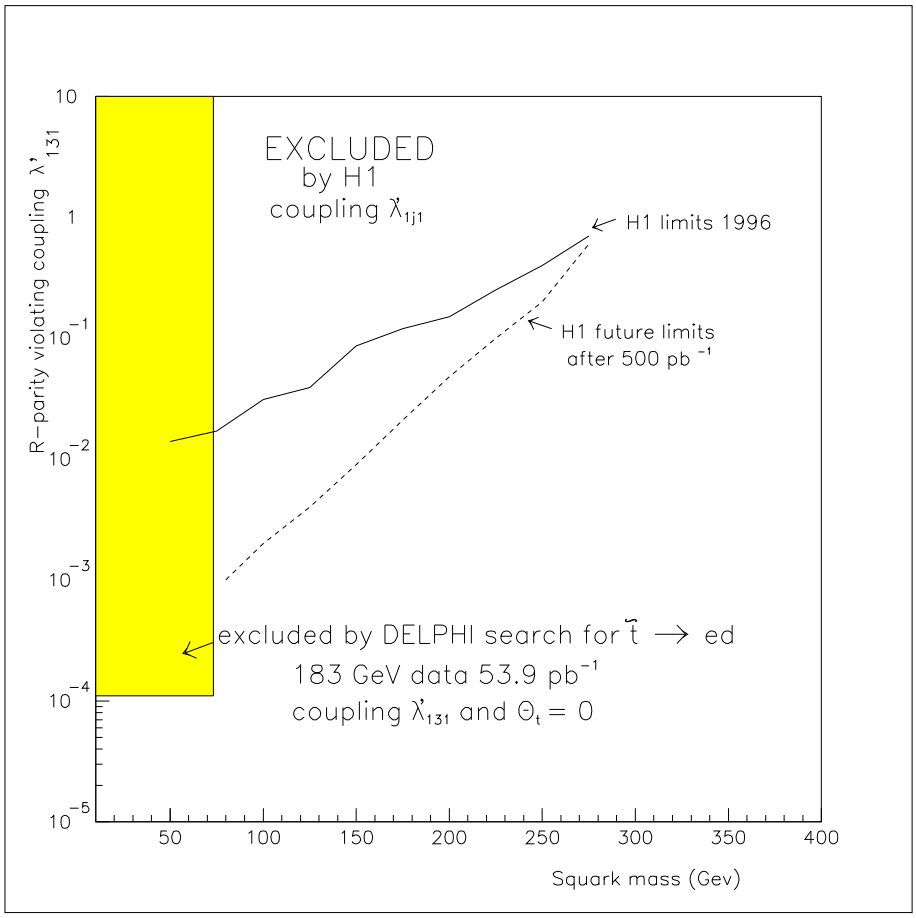

Figure 19: Stop searches with a dominant λ' coupling: exclusion domain in the λ'_{131} and $m_{\tilde{t}_1}$ in case of a pure left stop.

5 $\not{R}_p$ decays with a dominant λ'' coupling

In this section we treat the hadronic multijet events coming from the decay through the operators λ''_{ijk}. There will be 2 types of events in these topologies.

- Chargino and neutralino decays to multijet (more than 4 jets) topologies. Here only the 6 couplings of the first 2 columns of table 21 are accessible, since it is impossible to produce a top quark at LEP. Out of these, 4 involve a b in the decay products, giving 2 b's for the pair production. For these couplings, the b-tagging can be used to increase our sensitivity. If the lowest mass neutralino is the LSP it decays directly to 3 jets $\tilde{\chi}^0_1 \to udd$[7]. Its pair production gives a 6-jet topology. In the first analysis we search for peaks in the 6-jet topology. On the other hand the indirect decay of the chargino to the neutralino plus an off-shell W, giving a final 10-jet topology, is dominant in practically all the phase space, apart from cases of extreme degeneracy of the chargino and the neutralino. In these special cases the chargino decays directly in 3 jets and the first analysis can be transposed without any change. Another multijet topology is the production $\tilde{\chi}^0_1\tilde{\chi}^0_2$ decaying indirectly to 8 jets (5 jets for the $\tilde{\chi}^0_2$ and 3 jets for the $\tilde{\chi}^0_1$). The indirect decays of squarks to a quark and a neutralino and the subsequent decay of the neutralino to 3 jets will equally give 8-jet topologies. These 8-jet topologies will be considered in a future study.

- Squark direct decays to 4-jet topologies. The stop will decay to 2 down quarks ($\tilde{t} \to dd$) and the sbottom to an up and a down quark ($\tilde{b} \to ud$). For the case of the stop where the decay to a charm quark and a neutralino is naturally suppressed, the direct decay dominates for a large region of values of λ''. On the contrary the indirect decay of a sbottom to a b and $\tilde{\chi}^0_1$ dominates whenever it is kinematically possible. One then has 8-jet topologies as mentioned above.

final states	direct decay of	indirect decay of
$6j$ (*)	$\widetilde{\chi}^0_1\widetilde{\chi}^0_1$, $\widetilde{\chi}^0_2\widetilde{\chi}^0_1$, $\widetilde{\chi}^+_1\widetilde{\chi}^-_1$	
$6j + \not{E}$		$\widetilde{\chi}^0_2\widetilde{\chi}^0_1$
$6j + 2\,\mathrm{l}$		$\widetilde{\chi}^0_2\widetilde{\chi}^0_1$
$6j + 2\,\mathrm{l} + \not{E}$		$\widetilde{\chi}^+_1\widetilde{\chi}^-_1$
$8j$		$\widetilde{\chi}^0_2\widetilde{\chi}^0_1$
$8j + 1\,\mathrm{l} + \not{E}$		$\widetilde{\chi}^+_1\widetilde{\chi}^-_1$
$10j$ (*)		$\widetilde{\chi}^+_1\widetilde{\chi}^-_1$

Table 20: Final states in neutralino and chargino pair production when a UDD coupling is dominant. (*) denotes final states reconstructed in the multijet analysis.

[7] here d denotes a "down" and u an "up" quark

ijk	$\lambda''_{ijk} \leq$	ijk	$\lambda''_{ijk} \leq$	ijk	$\lambda''_{ijk} \leq$
$\lambda''_{uds}(112)$	10^{-6}	$\lambda''_{cds}(212)$	1.25	$\lambda''_{tds}(312)$	0.5
$\lambda''_{udb}(113)$	10^{-4}	$\lambda''_{cdb}(213)$	1.25	$\lambda''_{tdb}(313)$	0.5
$\lambda''_{usb}(123)$	1.25	$\lambda''_{csb}(223)$	1.25	$\lambda''_{tsb}(323)$	0.5

Table 21: Limits [10] on the $\not{R}_p$ couplings λ'' in units of ($m_{\tilde{f}}$/100 GeVcc), where $m_{\tilde{f}}$ is the appropriate sfermion mass.

5.1 Reconstructing masses in multijet (6-10) events

Mass reconstruction with a least 6 jets requires specific methods due to large jet multiplicity. The mass reconstruction is performed in three steps. First, we clusterize the hadronic event to the nominal number of jets needed i.e. 6, 8 or 10. For this we used the *ckern* package [38] based on the Cambridge clusterisation algorithm [39], which gives us, for each event, all the possible jet configurations between 2 and 10 jets and the DURHAM distance resolution $Y_{mn} \equiv y^{n \to m}$ corresponding to the transition value between the m and n jet configurations ($m > n$). The choice of this clustering algorithm is motivated by the fact that it is specially performant for mixed configurations with soft and hard jets. This is specially the case for our multijets analysis with the substructure due to the secondary decay of the $\tilde{\chi}_1^0$. The "soft freezing" procedure implemented in this algorithm which considers the least energetic one as final state jet and consequently tends to protect small jets from the nearest energetic jet. A better resolution of jet substructure is then obtained.

Associating each jet to its parent $\tilde{\chi}_1^0$ or $\tilde{\chi}_1^+$ is the most essential step in obtaining an adequate mass resolution. The choice of a smallest jet pairing difference used in the case of four jet topology is not applicable to multijets. Therefore we decided to use a neural network for this difficult task. The SNNS package [40] has been used with the standard backpropagation learning method. The configuration for the 6-jet neural network is 15 input nodes, 20 hidden nodes and 6 output nodes, while for 10-jet neural network it is 45 input nodes, 50 hidden nodes and 10 output nodes. For inputs we have chosen the 15 and 45 combinations of dijet invariant masses m_{ij}^2/s for 6 and 10 jets respectively. The training and validation patterns (20 000 each) are produced by a toy Monte Carlo where only decay and boost are implemented at the quark level. Two heavy objects with random masses in a 30 GeV/c^2 $\tilde{\chi}_1^0$ mass window for $\tilde{\chi}_1^0\tilde{\chi}_1^0$ and a 15 GeV/c^2 ($\tilde{\chi}_1^+$ mass) $\times$ 15 GeV/c^2 ($\tilde{\chi}_1^0$ mass) window for $\tilde{\chi}_1^+\tilde{\chi}_1^-$ production and subsequent indirect decay to $\tilde{\chi}_1^0$, are generated. The data are analysed separately in each mass window. After energy ordering, the output (6 and 10) nodes have the information of their parent heavy object. The training output node values are given in table 22.

The last remaining task is the 5C-6C fit on the jet momenta for 6 or 10 jets respectively. The 10-jet rescaling case is special in the sense that we can impose not only equal mass constraint on the 2 $\tilde{\chi}_1^\pm$ but also an equal mass constraint on the jet substructure i.e. the 2 $\tilde{\chi}_1^0$ produced by the 2 $\tilde{\chi}_1^\pm$ decays. This 5-6C fit algorithm is based on the multijets algorithm developped for the W mass reconstruction [41].

In order to test our mass reconstruction method, we apply it on different generated processes giving 6 and 10-jet topologies after full DELPHI simulation. The signals have

Jet index	1	2	3	4	5	6
Output node value	1	0	1	0	0	1

Jet index	1	2	3	4	5	6	7	8	9	10
Output node values	1	.8	0	.2	0	1	1	.8	.2	0

Table 22: Example of training values of the neural network associating jets to their parent heavy particle. Jets are ordered by decreasing energy. The first table shows the output training values for the 6-jet configuration: 1 means jet coming from the first $\tilde{\chi}_1^0$ and 0 for jet coming from the second $\tilde{\chi}_1^0$. The second table shows the output training values for the 10-jet configuration: 1 means that the jet is coming from the $\tilde{\chi}_1^0$ (3 over 5 jets) belonging to $\tilde{\chi}_1^+$. 0.8 means jet coming from W^{+*} (2 over 5 jets) belonging to the same $\tilde{\chi}_1^+$. 0 means that the jet is coming from the $\tilde{\chi}_1^0$ (3 over 5 jets) belonging to from $\tilde{\chi}_1^-$, 0.2 means jet coming from W^-* (2 jets over 5 jets) belonging to the same $\tilde{\chi}_1^-$.

been generated with SUSYGEN [18] and 1000 events are produced for each mass combination. Table 23 shows the different generated masses and the corresponding efficiency. Note the R-parity violating decay of squarks are generated with a λ''_{212} coupling equal to 0.1.

6-jet topologies						
$\tilde{\chi}_1^0$ mass GeV/c^2	15	22	38	52	68	80
ϵ (%)	44	50	57	53	46	25

10-jet topologies														
$\tilde{\chi}_1^+$ mass GeV/c^2	52				68					82				
$\tilde{\chi}_1^0$ mass GeV/c^2	10	22	38	48	10	22	38	52	64	22	38	50	68	78
ϵ (%)	21	24	25	29	27	27	34	36	25	32	37	38	42	35

Table 23: List of full simulation masses corresponding to characteristic topologies of $\tilde{\chi}_1^0$ and $\tilde{\chi}_1^+$ decays. Efficiency is given by the number of events in the window mass $m_{gen} \pm 4GeV/c^2$. For the 10 jet decays, only $\tilde{\chi}_1^+$ mass resolution is considered.

As it has been mentioned above, the mass reconstruction is performed in a 30 GeV/c^2 mass window for the 6 jet analysis and a 15×15 GeV/c^2 mass window for the 10 jet analysis. The main reason for these mass windows comes from the difference in the decays and consequently on the kinematics of the event between different $\tilde{\chi}_1^+$ and/or $\tilde{\chi}_1^0$ masses. We analysed the 183 GeV data in 14 mass windows for the indirect $\tilde{\chi}_1^+\tilde{\chi}_1^-$ decays and in 6 mass windows for $\tilde{\chi}_1^0\tilde{\chi}_1^0$ decays.

In what follows, we sum up the different cuts used in these analyses. The cuts concerning hadronic selection and rejection of initial state radiation events (ISR) are applied with the same values on each mass window analysis.

- **Hadronic selection:**
  - the charged multiplicity has to be greater or equal to 14;

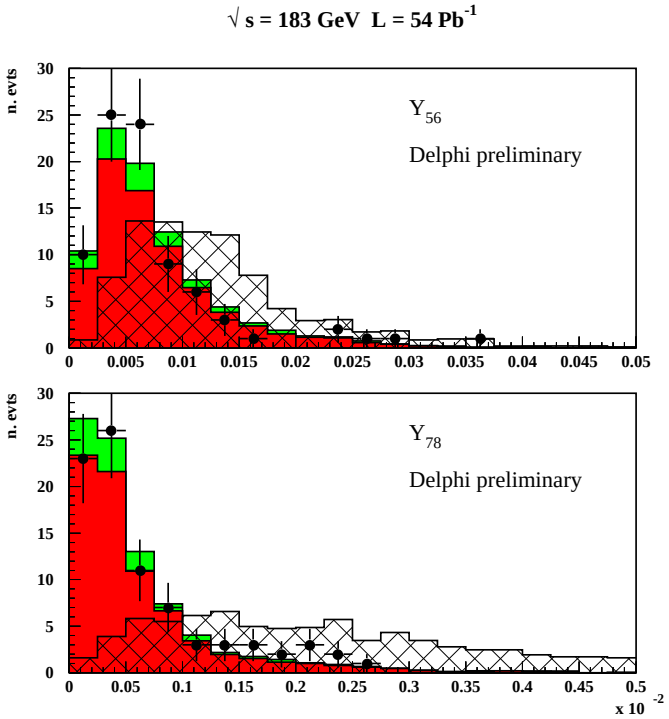

Figure 20: Neutralino and chargino analysis with λ'' couplings: distribution of Y_{56} Y_{78} Durham resolution variables used in the 6-jet (cut on Y_{56}) and 10-jet (cut on both Y_{56} and Y_{78}) topologies.The light grey histogram (green in colour) corresponds to the Z($q\bar{q}$) γ expected background. The dark grey histogram (red in colour) corresponds to the WW expected background. Data are shown in black dots. The hatched histogram shows the signal ($\tilde{\chi}_1^0\tilde{\chi}_1^0$ with $m_{\tilde{\chi}^0} = 38$ GeV/c^2 and $\tilde{\chi}_1^+\tilde{\chi}_1^-$ with $m_{\tilde{\chi}^\pm} = 68$ GeV/c^2) normalized to 2 pb.

  - the total event energy is required to be greater than $0.30 \times \sqrt{s}$;
  - the total energy from neutral particles is required to be greater than $0.30 \times \sqrt{s}$.

- **Selection against ISR events:**
  - the energy of the most energetic photon in the event must be less than 35 GeV;
  - the missing momentum must be less than 45 GeV/c;
  - examining the 3-jet topology, the electromagnetic energy of each jet has to be less than 90% of the jet energy and the charged multiplicity of each jet has to be at least 2.
- **W mass cut:**
  - examining the 4-jet topology, a specific 5C fit is applied and $M_{5C}^{4jets} < 70$ GeV/c^2 is required. This cut is applied only for signal searches with $\tilde{\chi}_1^0$ or $\tilde{\chi}^\pm$ masses < 60 GeV/c^2.

Figure 20 shows data and MC agreement after the W-mass cut on the 6 and 8 jet Y_{56} and Y_{78} Durham resolution variables with a $\tilde{\chi}_1^+\tilde{\chi}_1^-$ signal normalised to 2 pb ($m_{\tilde{\chi}^\pm} = 68$ GeV/c^2 and $m_{\tilde{\chi}^0} = 38$ GeV/c^2).

The following cuts, concerning events which can be classified as events with more than 4-jets, are different for each mass window analysis due to their sensitivity to the kinematics (i.e to the chargino and neutralino masses), therefore only the description of

the cuts is reported here.

- **Selection of events with more than 4-jets:**
  - *Oblatness* cut for event sphericity coming from the major and minor axis of the sphericity;
  - *4-jet cut* : cut on the Durham resolution variable $Y_{34}(y^{4\to3})$ transition value from 4 to 3 jet topology;
  - *5-jet cut* : remaining events are selected with respect to their values on the variables $\alpha^5_{min} \times E^5_{min}$ and $\beta^5_{min} \times E^5_{max}/E^5_{min}$ where α_{min} is the minimum angle between the 5 jets, β_{min} is the minimum angle between the highest energetic jet and the four others and E_{max} (E_{min}) is the maximum (minimum) jet energy [30];
  - *6-jet cut* : cut on the product $\alpha^6_{min} \times E^6_{min}$ for the 6 jets. The meaning of the variables is explained in the *5-jet cut*. This cut is applied in the 6 (10-jet topologies), where the generated $\tilde{\chi}^0_1$ ($\tilde{\chi}^+_1$) have masses > 75 GeV/c^2. A cut on the Durham resolution variable $Y_{56}(y^{6\to5})$, transition value from 6 to 5 jet topology is also applied;
  - *8-jet cut* : cut on the Durham resolution variable $Y_{78}(y^{8\to7})$ transition value from 8 to 7 jet topology. This cut is applied only on $\tilde{\chi}^+_1\tilde{\chi}^-_1 \to$ 10-jet analysis.

Signal efficiency is obtained counting the number of expected signal events with a fitted mass in the 8 GeV/c^2 range around the generated mass, which corresponds to $m_{gen} \pm 4$ GeV/c^2. Then we make the assumption in what follows that this efficiency is constant in the 15 GeV/c^2 $\times$ 15 GeV/c^2 ($\tilde{\chi}^+_1$,$\tilde{\chi}^0_1$) mass window which corresponds to a small efficiency extrapolation of 3.5 GeV/c^2 for each side of the mass window analysis.

After cuts the efficiency of the 6-jet analysis is constant to 15 % for masses up to 75 GeV/c^2 and goes down to 8 % in the W mass region. The efficiency of the 10-jet analysis is around 10 % for $\tilde{\chi}^+_1$ with masses between 45 and 70 GeV/c^2 and 15 % for $\tilde{\chi}^+_1$ with masses between 75 and 90 GeV/c^2. The dominant background for light (heavy) charginos is the QCD (WW) background. The number of remaining events in the real data, SM background as well as the efficiencies obtained in the 6, 10-jet analyses are reported in table 24. The experimental cross section (σ_{excl}) that can be excluded at 95 % confidence level, is obtained by counting the number of real data and expected background events, in each 8 GeV/c^2 $\tilde{\chi}^+_1$ mass range. The σ_{excl} as well as the N_{95} number of expected signal events is also reported on the table 24.

Figure 21 shows the chargino mass fitted in 10-jets analysis for the data, the background and for a signal normalised to 2 pb.

Note that in this analysis (λ''_{212} coupling), no assumption on the quark flavour has been made. Searches of λ'' couplings which lead to the production of one or several b quarks, have the advantage of using b-tagging techniques and have better sensitivity. Therefore we can safely assume that our results obtained for the λ''_{212} are valid for the 5 other $\lambda''_{ijk}, i \neq 3$ couplings as well.

5.2 Stop and sbottom search

In this search, the direct decay of stop and sbottom squarks through the $\lambda''_{tsb}(323)$ and $\lambda''_{usb}(123)$ couplings was considered. In case of stop (sbottom) pair production, the final states contain 2 (none) b quarks and the analysis is the same as the one reported in section 4.2 for the sneutrino decay through λ'_{313} (λ'_{311}) coupling. Stop (sbottom) signals

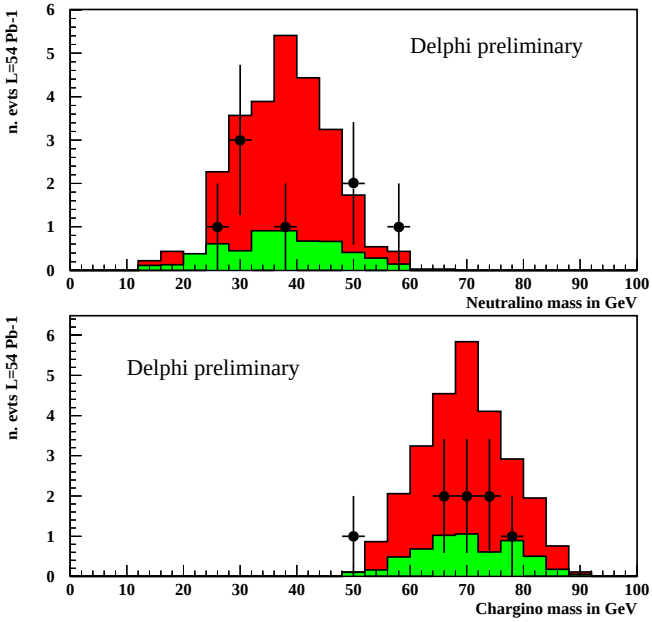

Figure 21: Reconstructed $\tilde{\chi}_1^0$ and $\tilde{\chi}_1^+$ in the 10-jet analysis. Data are shown in black dots. The light grey histogram (green in colour) corresponds to the expected background. The dark grey (red in colour) histogram, shows the signal (indirect decay of $\tilde{\chi}_1^+\tilde{\chi}_1^- \rightarrow$ 10 jets with $m_{\tilde{\chi}^\pm} = 68$ GeV/c^2 and $m_{\tilde{\chi}^0} = 38$ GeV/c^2), normalized to 2 pb.

were simulated at different masses in the range of 55-80 GeV/c^2, for two mixing angles corresponding to maximal ($\theta_t = 56^0$, $\theta_b = 40^0$) and minimal ($\theta_{t,b} = 0^0$) mixing. The efficiencies obtained as a function of the generated stop masses for $\lambda''_{tsb}(323)$ are given in table 25. These results are also valid for stop decay via $\lambda''_{tdb}(313)$ coupling and sbottom decay via $\lambda''_{cdb}(213)$, $\lambda''_{csb}(223)$ couplings.

5.3 Interpretation of λ'' dominant searches in terms of MSSM parameters

No excess has been seen in data with respect to the expected SM background. Combining the 6-jet analysis (used for the direct decay of $\tilde{\chi}_1^+\tilde{\chi}_1^-$ or $\tilde{\chi}_1^0\tilde{\chi}_1^0$) and the 10-jet analysis (used for indirect decay of $\tilde{\chi}_1^+\tilde{\chi}_1^-$) results, an exclusion contour in μ, M_2 plane at 95 % confidence level has been derived for different values of m_0 (90 and 300 GeV/c^2) and tanβ (1.5 and 90). The μ, M_2 exclusion plot is obtained with a 1 GeV step for μ and 2 GeV step for M_2. Note that, as already mentioned in section 4.1.3, LEP1 results cover regions where the charginos are lighter than 45 GeV/c^2 therefore no specific study on charginos with masses lower than this value, has been performed. Inside the excluded area, some regions are not covered in case of $m_0 = 90$ and tan$\beta = 1.5$, due to the low $\tilde{\chi}_1^+\tilde{\chi}_1^-$ cross section for small M_2 values and negative μ values. Complementary searches on $\tilde{\chi}_2^0$ $\tilde{\chi}_1^0$ process could cover these regions.

For the stop and sbottom squarks a preliminary limit at 95% confidence level is calculated for the $\lambda''_{tsb}(323)$ and the $\lambda''_{usb}(123)$ terms. Stop masses lower than 76(73) GeV/c^2 for mixing angle $\theta_t = 0^0(56^0)$ and sbottom masses lower than 74(62) GeV/c^2 for mixing angle

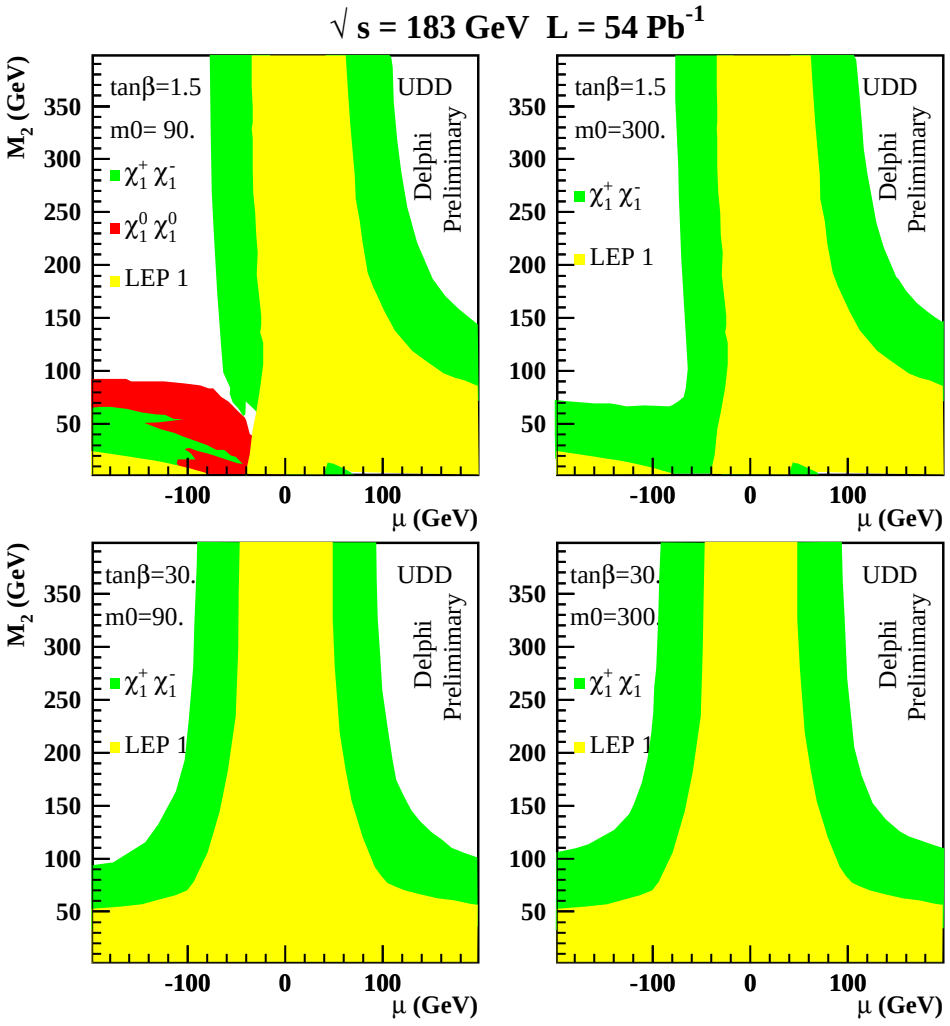

Figure 22: exclusion plot in μ, M_2 plan for $\tilde{\chi}_1^0\ \tilde{\chi}_1^0$ and $\tilde{\chi}_1^+\ \tilde{\chi}_1^-$ production in the case of a dominant UDD R-parity violation coupling.

$\theta_b = 0^0(40^0)$ are excluded. The results derived from stop searches through the $\lambda''_{tsb}(323)$ coupling are also valid for $\lambda''_{tdb}(313)$ term, whereas results from sbottom searches through the $\lambda''_{usb}(123)$ coupling are also valid for $\lambda''_{udb}(113)$, $\lambda''_{cdb}(213)$ terms.

6 jet topologies						
$m_{\tilde{\chi}_1^0}$	15	22	38	52	68	80
Window	5-15	15-30	30-45	45-60	60-75	75-90
ϵ (%)	19	15	17	14.2	17.6	8.6
SM	7.53	5.20	2.60	5.90	5.40	14.00
Data	4	9	4	5	5	12
N_{95}	4.85	10.79	7.01	6.47	6.47	8.09
σ (excl.) (pb)	0.46	1.32	0.75	0.83	0.67	1.73

10 jet topologies														
$m_{\tilde{\chi}_1^+}$	52	52	52	52	68	68	68	68	68	82	82	82	82	82
Window	45-60	45-60	45-60	45-60	60-75	60-75	60-75	60-75	60-75	75-92	75-92	75-92	75-92	75-92
$m_{\tilde{\chi}_1^0}$	10	22	38	48	10	22	38	52	64	22	38	50	68	78
Window	5-15	15-30	30-45	45-55	5-15	15-30	30-45	45-60	60-70	15-30	30-45	45-60	60-75	75-85
ϵ (%)	6.8	8.6	10.5	11	8.8	9.5	9.6	9.7	5.9	14	14.1	14.4	11.8	13.5
SM	6.02	0.93	1.82	6.60	9.06	4.34	2.14	2.22	5.09	2.61	0.69	2.68	2.56	13.88
Data	8	2	2	6	5	4	3	2	5	2	0	2	1	7
N_{95}	9.20	5.94	5.40	6.48	5.40	5.94	5.94	4.86	6.48	4.86	3.24	4.86	3.78	5.39
σ_{excl} (pb)	2.5	1.26	0.94	1.08	1.35	1.04	1.13	0.93	2.01	0.63	0.42	0.63	0.59	0.73

Table 24: Remaining data, expected SM background (W^+W^-, QCD and ZZ) for each mass window of the 6 and 10 jet analyses. The corresponding signal efficiency, N_{95} and $\sigma_{excl.}$ are given.

$m_{\tilde{t}}(\lambda''_{tsb})$	55 GeV/c^2 eff.(%)			60 GeV/c^2 eff.(%)			65 GeV/c^2 eff.(%)			70 GeV/c^2 eff.(%)			75 GeV/c^2 eff.(%)		
E_{CM} (GeV)	161	172	183	161	172	183	161	172	183	161	172	183	161	172	183
$\theta_t = 0^0$	39	39	40	39	40	41	38	42	40	42	44	40	48	48	42
$\theta_t = 56^0$	36	40	40	38	40	40	40	39	38	43	42	40	49	47	44

Table 25: The efficiency as a function of the $\tilde{t}_1$, mass after all cuts at center of mass energy of 161, 172 and 183 GeV for $\theta_t = 0, 56^0$. Both of the efficiencies are similar due to the same final states.

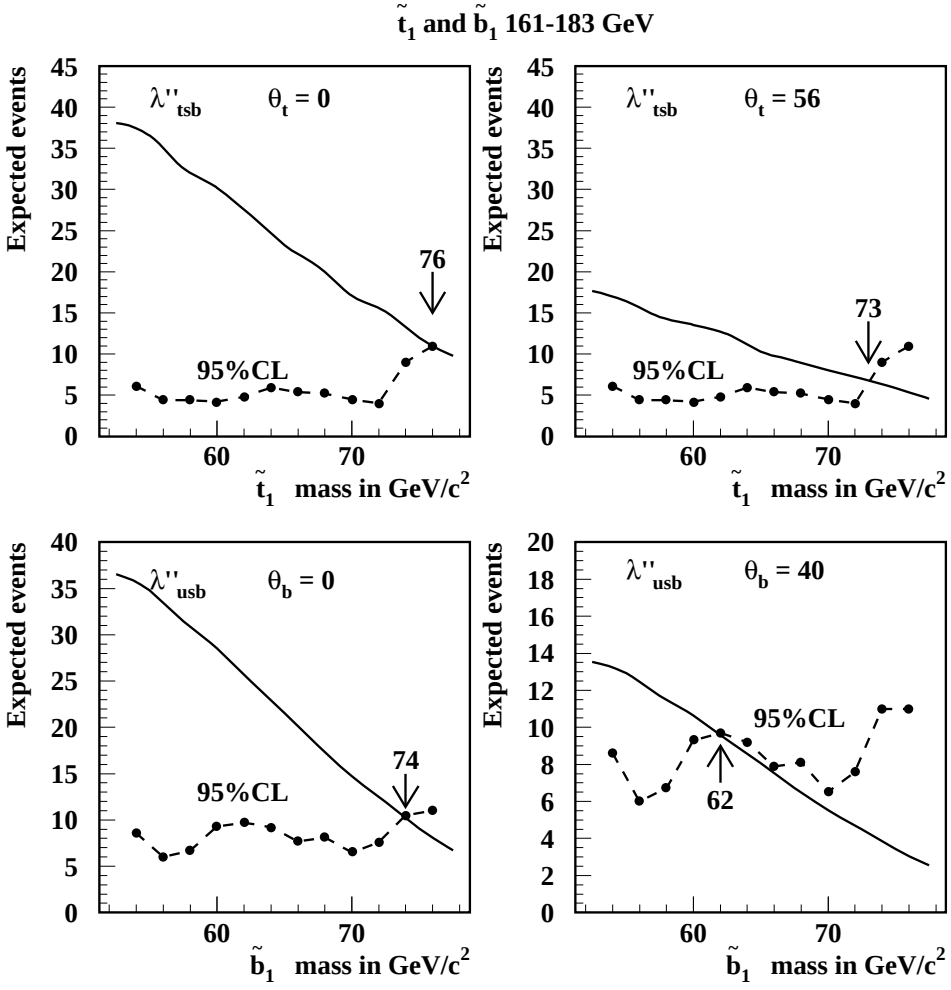

Figure 23: Stop and sbottom analysis with λ''_{UDD} couplings: Expected events (dots connected with a dotted line) versus mass at 95% for the $\lambda''_{tsb}(323)$ and the $\lambda''_{usb}(123)$ terms for maximal and minimal mixing angles. The solid line represents the number of expected events from the MSSM cross section taking into account the integrated luminosity and the efficiency at each center of mass energy.

6 Conclusion

Searches for $\not{R}_p$ effects in e^+e^- collisions at $\sqrt{s} = 183$ GeV have been performed with the DELPHI detector. The pair production of neutralinos, charginos and sfermions has been studied for several types of λ, λ' and λ'' operators with the assumption that the LSP has a negligible lifetime. No evidence for R-parity violation has been observed so far, therefore limits have been set within the MSSM framework, as summarized below.

Direct and indirect decays of sparticles via λ_{122} and λ_{133} terms have been analysed, giving the following results, valid for all λ couplings:

- from neutralino and chargino study, $m_{\tilde{\chi}^0} > 27$ GeV/c^2 and $m_{\tilde{\chi}^\pm} > 89$ GeV/c^2;
- from charged slepton study, the most conservative limit $m_{\tilde{l}} > 61$ GeV/c^2 is obtained from the results of direct $\not{R}_p$ decay;
- from sneutrino study, the most conservative limit $m_{\tilde{\nu}} > 62$ GeV/c^2 is obtained from the results of indirect $\not{R}_p$ decay.

The study of direct and indirect decays of neutralinos and charginos via λ'_{1jk} on one hand and $\lambda''_{ijk}, i \neq 3$ on the other, allowed to constrain the MSSM parameter space extending the region excluded by LEP1.

Limits on sneutrino, charged slepton and stop masses were obtained considering the direct decay via λ' coupings:

- $m_{\tilde{\nu}_\tau} > 76$ GeV/c^2 for λ'_{333}, ;
- $m_{\tilde{\nu}_\tau} > 72$ GeV/c^2 for λ'_{313}, valid also for λ'_{3jk}, $j \neq k$ and either $j = 3$ or $k = 3$;
- $m_{\tilde{\nu}_\tau} > 60$ GeV/c^2 and $m_{\tilde{\tau}} > 71$ GeV/c^2 for λ'_{311}, valid also for λ'_{3jk}, $j, k \neq 3$;
- $m_{\tilde{t}} > 73$ GeV/c^2 for λ'_{131}, valid also for λ'_{13k};
- $m_{\tilde{t}} > 81$ GeV/c^2 for λ'_{231}, valid also for λ'_{23k}.

The stop (sbottom) direct decays via λ''_{323} (λ''_{123}) gave lower limit on squark masses:

- $m_{\tilde{t}} > 76(73)$ GeV/c^2 for mixing angle $\theta_t = 0^0(56^0)$, valid also for λ''_{313};
- $m_{\tilde{b}} > 74(62)$ GeV/c^2 for mixing angle $\theta_b = 0^0(40^0)$, valid also for $\lambda''_{ij3}, i, j \neq 3$.

Acknowledgements

We are greatly indebted to our technical collaborators and to the funding agencies for their support in building and operating DELPHI detector. We are particularly thankful to the members of the CERN-SL Division for the excellent performance of LEP during the high energy run of 1997.

References

[1] For reviews, see e.g. H.P. Nilles, *Phys. Rep.***110** (1984) 1; H.E. Haber and G.L. Kane, *Phys. Rep.* **117** (1985) 75.

[2] P. Fayet, *Phys. Lett.* **B69** (1977) 489; G. Farrar and P. Fayet, *Phys. Lett.* **B76** (1978) 575.

[3] S. Weinberg, *Phys. Rev.* **D26** (1982) 287.

[4] I. Hinchliffe and T. Kaeding, *Phys. Rev.* **D47** (1993) 279.

[5] C.E. Carlson et al., *Phys. Lett.* **B357** (1995) 99.

[6] S. Dawson, *Nucl. Phys.* **B261** (1985) 297.

[7] H. Dreiner and G.G. Ross, *Nucl. Phys.* **B365** (1991) 597.

[8] V. Barger, G.F. Guidice, T. Han, *Phys. Rev.* **D40** (1989) 2987.

[9] H. Dreiner, hep-ph/9707435.

[10] G. Bhattacharyya, hep-ph/9709395 and *Nucl. Phys.***B** *(Proc. Suppl.)* **52A** (1997) 83.

[11] P. Abreu et al., *Nucl. Instr. Meth.* **378** (1996) 57.

[12] T. Sjostrand, *Computer Phys. Comm.* **39** (1986) 347.

[13] F.A. Berends, R. Kleiss, R. Pittau, *Computer Phys. Comm.* **85** (1995) 437.

[14] F.A. Berends, P.H. Davervelt, R. Kleiss, *Computer Phys. Comm.* **40** (1986) 271,285 and 309.

[15] S. Nova, A. Olshevski, T. Todorov, DELPHI 90-35 PROG 152.

[16] S. Jadach, Z. Was, *Computer Phys. Comm.* **79** (1994) 503.

[17] J.E. Campagne, R. Zitoun, *Zeit. Phys.* **C43** (1989) 469.

[18] S. Katsanevas, P. Morawitz, hep-ph/9711417, sumbitted to Comp. Phys. Comm.

[19] M. Berggren, P. Billoir and M.A. Do Vale, SGV 1.0 Simulation à Grande Vitesse, unpublished.

[20] S. Catani et al., *Phys. Lett.* **B269** (1991) 432.

[21] M. Berggren, M. Gandelman, J.H.Lopes, DELPHI 97-156 PHYS 735.

[22] Particle Data Group, *Phys. Rev.* **D54** (1996) 1.

[23] J. Erler, J.L. Feng and N. Polonsky, *Phys. Rev. Lett.* **78** (1997) 3063.

[24] T. Kon, T. Kobayashi and S. Kitamura, ITP-SU-94/01.

[25] M. Besançon and Ph. Gris, DELPHI 96-25 PHYS 600.

[26] K. Hikasa and M. Kobayashi, *Phys. Rev.* **D36** (1987) 724.

[27] J. Kalinowski, R. Rückl, H. Spiesberger and P.M. Zerwas *Zeit. Phys.* **C74** (1997) 595.
E. Perez, Y. Sirois and H. Dreiner, Proceedings of the Workshop "Future Physics at HERA", hep-ph/9703444.
G. Altarelli, J. Ellis, G.F. Giudice, S. Lola and M.L. Mangano CERN *Nucl. Phys.* **B506** (1997) 3.

[28] K. Mönig, DELPHI 97-174 PHYS 748.

[29] N.J.Kjaer, R.Moller, DELPHI 91-17 PHYS 88.

[30] P.Bambade et al., DELPHI 97-51 PHYS 703.

[31] A. Ballestrero et al., *Zeit. Phys.* **C74** (1997) 493.

[32] G.V.Borisov,C.Mariotti, DELPHI 97-16 PHYS 672.

[33] M. Jimbo, T. Kaneko and T. Kon, MINAMI-TATEYA collaboration, TMCP-95-1.

[34] S. Kawabata, *Computer Phys. Comm.* **41** (1986) 127.

[35] M. Drees and K.I. Hikasa, *Phys. Lett.* **B252** (1990) 127.

[36] P. Gris, DELPHI 97-54 PHYS 704.

[37] W. Adam et al., DELPHI 97-22 PHYS 678.

[38] S. Bentvelsen and I. Meyer, hep-ph/9803322, submitted to *Eur. Phys. J.***C**. The *ckern* package can be found on wwcn1.cern.ch/~ stamb/ckern/ckern.html

[39] Yu.L. Dokshitzer, G.D. Leder, S. Moretti, B.R. Webber *J. High Energy Phys.***08** (1997) 001.

[40] Stuttgart Neural Network Simulator User manual, version 4.1
http://www-ra.informatik.uni-tuebingen.de/SNNS/

[41] A. Duperrin, DELPHI 97-170 PHYS 745.